INDOOR LOCALIZATION BASED ON ROUND-TRIP TIME OF BLUETOOTH LOW ENERGY BEACONS

BY

SUPATANA HENGYOTMARK

A THESIS SUBMITTED IN PARTIAL FULFILLMENT OF
THE REQUIREMENTS FOR THE DEGREE OF MASTER OF
ENGINEERING (INFORMATION AND COMMUNICATION
TECHNOLOGY FOR EMBEDDED SYSTEMS)
SIRINDHORN INTERNATIONAL INSTITUTE OF TECHNOLOGY
THAMMASAT UNIVERSITY
ACADEMIC YEAR 2016

INDOOR LOCALIZATION BASED ON ROUND-TRIP TIME OF BLUETOOTH LOW ENERGY BEACONS

BY

SUPATANA HENGYOTMARK

A THESIS SUBMITTED IN PARTIAL FULFILLMENT OF
THE REQUIREMENTS FOR THE DEGREE OF MASTER OF
ENGINEERING (INFORMATION AND COMMUNICATION
TECHNOLOGY FOR EMBEDDED SYSTEMS)
SIRINDHORN INTERNATIONAL INSTITUTE OF TECHNOLOGY
THAMMASAT UNIVERSITY
ACADEMIC YEAR 2016

INDOOR LOCALIZATION BASED ON ROUND-TRIP TIME OF BLUETOOTH LOW ENERGY BEACONS

A Thesis Presented

By

SUPATANA HENGYOTMARK

Submitted to

Sirindhorn International Institute of Technology

Thammasat University

In partial fulfillment of the requirements for the degree of

MASTER OF ENGINEERING (INFORMATION AND COMMUNICATION

TECHNOLOGY FOR EMBEDDED SYSTEMS)

Approved as to style and content by

Advisor and Chairperson of Thesis Committee

(Asst. Prof. Dr. Teerayut Horanont)

Committee Member and
Chairperson of Examination Committee

(Dr. Kamol Kaemarungsi)

Committee Member

(Prof. Dr. Kazuhiko Fukawa)

Committee Member

(Dr. Virach Sornlertlamvanich)

AUGUST 2017

i

Abstract

INDOOR LOCALIZATION BASED ON ROUND-TRIP TIME OF BLUETOOTH
LOW ENERGY BEACONS

by

SUPATANA HENGYOTMARK

Bachelor of Engineering (Civil Engineering), Chulalongkorn University, 1998

Master of Engineering (Structural Engineering), Chulalongkorn University, 2001

Master of Engineering (Information and Communication Technology for Embedded
Systems), Sirindhorn International Institute of Technology, Thammasat University,
2017

Indoor localization system is becoming widespread due to an increasing
demand on location-based services. Many researchers are seeking for techniques to
improve its accuracy and reliability. Pseudo-ranging is a fundamental and essential
process in all positioning systems. For indoor positioning systems, many mediums can
be utilized such as sound, light or radio wave. Bluetooth Low Energy (BLE) has gained
a popularity from many researchers in recent years for ranging, in which most of them
rely on Received Signal Strength Indicator (RSSI) of the broadcasting beacons. The
significant shortcoming of the RSSI is that it is highly sensitive, even with a slight
change, to the surroundings or the orientation of the device. In this thesis, the
positioning system based on the two-way Time-of-Flight (ToF) approach for ranging
of BLE beacons has been proposed. The Round-Trip Time (RTT) of the beacons has
been measured and the pseudo-ranging calculation has been subsequently performed.
The RTT is measured by CPU clock cycle of the scanner after sending the scan request
packet to the advertiser, and then waiting for the scan response packet to end the time
measurement. The external Temperature Compensated Crystal Oscillator (TCXO) is

also introduced for reducing the uncertainty of clock drift. The method for avoiding the collision of the concurrent scan request packets has been proposed. The real-time tracking application framework has also been implemented, and the two trilateration approaches are considered. The pseudo-ranging results show that the relationship between the RTT and distance tends to be linear. The study results also indicate that the accuracy can be improved by considering the RTT from the advertising channel that gives the best RSSI. The estimated positions from the proposed framework give a discrepancy less than 1 meter regardless of what the tracking object is stationary or on moving.

Keywords: Bluetooth Low Energy, Indoor Localization, Indoor Positioning, Round-Trip Time

Acknowledgements

Table of Contents

sList of Tables

List of Figures

Chapter 1

Introduction

1.1 Background

The Global Navigation Satellite System (GNSS) has proven itself to provide a precise positioning accuracy for many outdoor applications. However, its signal cannot penetrate into the building. This leads many researchers to develop indoor positioning systems by utilizing various mediums such as sound, light or radio wave to achieve pseudo-ranging and later on performing positioning calculation.

Bluetooth Low Energy (Bluetooth LE or BLE) is one of the most famous mediums used for indoor positioning systems. It has been part of Bluetooth Core Specifications [1] since the release of version 4.0, which mostly aims for sensor devices that periodically advertise data beacons with a very low power consumption. BLE can be found in almost all of smart phones nowadays. It has been widely used in indoor positioning due to low cost, less effort for implementation, and low power consumption. However, due to a lack of precise time synchronization in BLE, it is difficult to determine pseudo-ranging by Time-of-Flight (ToF) approach such as Time-of-Arrival (ToA) or Time-Difference-of-Arrival (TDoA). Moreover, Angle-of-Arrival (AoA) approach requires directional or antenna array, which is rarely found in BLE device [2]. Therefore, almost all researches using BLE for ranging have been paid attention to Received Signal Strength Indicator (RSSI) of the beacons.

This thesis proposes the indoor localization system for real-time tracking application. The pseudo-ranging is evaluated from Round-Trip-Time (RTT) of BLE beacons. The RTT is measured from a travel time of a scan request packet (SCAN_REQ) after sending and receiving a corresponding response (SCAN_RSP) by using CPU clock cycle. The scan request and response features are a well-established protocol defined in [1]. The distance is then determined from the RTT-distance relationship. After obtaining enough distances, the estimated position is calculated using trilateration technique, and the result is then shown in the application.

1.2 Motivation

The demand on indoor positioning is increasing based on the emergence of location-based services in smartphone. Even though there are other systems that claimed a centimeter accuracy such as positioning system using a radio technology called ultra-wideband (UWB), it comes at a cost of hardware and, more importantly, it bothers users to implement. Wi-Fi and Bluetooth are commonly found in most smartphones nowadays. Most RF-based positioning systems rely on these things. Bluetooth becomes popular since its low energy sub-system (BLE) has been implemented. This thesis uses BLE technology in the positioning system due to its low-cost, low energy and availability in most smartphones.

1.3 Limitations

The major part in this thesis is pseudo-ranging by RTT of BLE beacon. The multipath fading can be encountered during measurement, which can cause error in packet being transmitted or received. This thesis checks only CRC for correctness of the packet rather than remedying the multipath fading directly. Besides, only two-dimensional space of positioning system is considered in this thesis

1.4 Outline

The rest of this thesis is organized in the following manner:

- **Chapter 1** introduces various techniques of positioning systems, motivation and limitation of this thesis.

- **Chapter 2** reviews works by other researchers related to general positioning technique as well as technique used in BLE.

- **Chapter 3** presents localization algorithms used in the positioning system.

- **Chapter 4** introduces BLE technology and describes pseudo-ranging technique from RTT of BLE beacon as well as a brief introduction of Kalman filter.

- **Chapter 5** proposes various services running on server dedicated for real-time tracking application framework.

Ref. code: 25595722040531NSG

- **Chapter 6** conducts experiments on pseudo-ranging, packet response rate, Kalman filter and positioning test.

- **Chapter 7** concludes this thesis and presents further study.

Chapter 2
Literature Review

2.1 General Positioning Techniques

Many technologies has been proposed for an indoor positioning system instead of a well-established GNSS. Each technology differs in coverage range, accuracy and cost as overview in [3] [4] [5]. In RF-based pseudo-ranging, It can be generally divided into four methods depending on the technique used i.e. ToF, AoA and RSSI. In ToF method, a travel time is determined by comparing a local time of the receiver with the timestamp in packet since it starts to transmit, and therefore this requires a precise time synchronization. The travel time is then converted to a distance if the speed of the signal is known. AoA method measures angle of incoming signals, in which its method requires a directional or antenna array so that the position can be calculated by using simple trigonometry. Since BLE lacks both precise time synchronization and directional or antenna array, the RSSI seems to be a highly applicable technique for BLE. The details of this is explained in the next section.

2.2 BLE Positioning Techniques

BLE-based positioning system mostly relies on the RSSI[2][6]. Pseudo-ranging is then obtained from the relationship between the RSSI and displacement that can be created from a radio propagation lost equation or experimentation [7]. Alternatively, a pre-defined mapping or fingerprinting of RSSI [8] [9] can also be used to determine the position. The significant shortcoming of the RSSI-based positioning is that it is highly sensitive, even with a slight change, to the surroundings or the orientation of the device.

The Round-Trip Time (RTT) has also been used for ranging because of its advantage as there is no need to perform time synchronization. However, this method introduces another source of error called internal node delay that comes from internal processing of the device. The additional node is used as a reference to estimate such internal delay [10]. This was done with Wi-Fi protocol by modifying a device driver of an operating system in order to reduce the internal processing time.

4

Since BLE signal is a radio wave that travels at speed of light, it therefore needs a high clock resolution in order to measure ToF. The concept of utilizing CPU clock cycle of microprocessor as a stopwatch to measure ToF has been proposed in [11]. This might be a problem in microcontroller to achieve that high resolution. Nevertheless, a reason making ToF possible to be measured is that the modern microcontroller has integrated the RF front-end as its peripheral into a single chip. This leads to the capability to control sending and receiving states as well as the ability for hardware interrupt at low-level. This helps reducing internal delay and estimating the travel time in a more predictable way.

Chapter 3
Localization Algorithms

There are several techniques to estimate or locate a position. In RF-based positioning, it can be classified into the method that utilizes RSSI, ToF and AoA as previously reviewed in Chapter 2. This chapter focuses on the 2D displacement-based positioning, which can be found using either RSSI or ToF. Nonetheless, its technique can also be further extended to application in a 3D problem. Three displacement-based positioning methods, known as trilateration, are described in the following sections.

3.1 Circle Intersection Method

Once enough distances from pseudo-ranging have been obtained, the next step is to compute the position from intersection point of circles as shown in Figure 3.1.
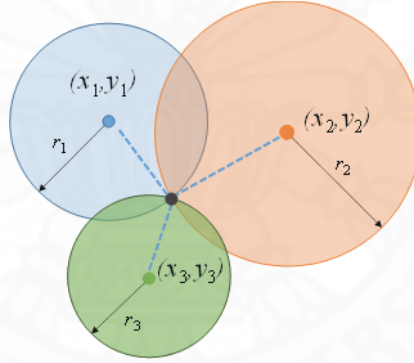
Figure 3.1 Three circle intersection.

This method involves with solving non-linear simultaneous equations, which are expressed as follows:

$$(x - x_1)^2 + (y - y_1)^2 = r_1{}^2$$
$$(x - x_2)^2 + (y - y_2)^2 = r_2{}^2 \qquad (3.1)$$
$$(x - x_3)^2 + (y - y_3)^2 = r_3{}^2$$

(x_i, y_i), r_i are center points and radius of the ith circle, respectively, where $i = 1 \ldots 3$.

6

Solving the non-linear equations is more complicated than the linear ones. Therefore, these non-linear equations are transformed into the linear system[12].

Equation (3.1) is rewritten into a general form as

$$(x - x_i)^2 + (y - y_i)^2 = r_i^2 \quad ; i = 1 \ldots n \tag{3.2}$$

The jth terms of x and y variable are introduced. Hence

$$\left(x - x_j + x_j - x_i\right)^2 + \left(y - y_j + y_j - y_i\right)^2 = r_i^2 \quad ; i = 1 \ldots n \tag{3.3}$$
$$j = 1 \ldots n$$

After expanding and rearranging terms in (3.3), it leads to

$$\left(x - x_j\right)(x_i - x_j) + \left(y - y_j\right)(y_i - y_j)$$
$$= \frac{1}{2}\left[\left(x - x_j\right)^2 + \left(y - y_j\right)^2 - r_i^2 + \left(x_i - x_j\right)^2 + \left(y_i - y_j\right)^2\right] \tag{3.4}$$

Substitute (3.2) into (3.4)

$$\left(x - x_j\right)(x_i - x_j) + \left(y - y_j\right)(y_i - y_j)$$
$$= \frac{1}{2}\left[r_j^2 - r_i^2 + d_{ij}^2\right] \tag{3.5}$$
$$= b_{ij}$$

where $d_{ij}^2 = \left(x_i - x_j\right)^2 + \left(y_i - y_j\right)^2 = $ distance between point i and j and

Let $j = 1$ and expand (3.5) for $i = 2 .. n$

$$(x - x_1)(x_2 - x_1) + (y - y_1)(y_2 - y_1) = b_{21}$$
$$(x - x_1)(x_3 - x_1) + (y - y_1)(y_3 - y_1) = b_{31}$$
$$(x - x_1)(x_4 - x_1) + (y - y_1)(y_4 - y_1) = b_{41} \tag{3.6}$$
$$\vdots$$
$$(x - x_1)(x_n - x_1) + (y - y_1)(y_n - y_1) = b_{n1}$$

The above equation is the linear system which can be easily rewritten in a matrix form as

7

$$\begin{bmatrix} x_2 - x_1 & y_2 - y_1 \\ x_3 - x_1 & y_3 - y_1 \\ x_4 - x_1 & y_3 - y_1 \\ \vdots & \vdots \\ x_n - x_1 & y_n - y_1 \end{bmatrix} \begin{pmatrix} x - x_1 \\ y - y_1 \end{pmatrix} = \begin{pmatrix} b_{21} \\ b_{31} \\ b_{41} \\ \vdots \\ b_{n1} \end{pmatrix} \tag{3.7}$$

or $$\mathbf{Ax} = \mathbf{b}$$

This system has $n - 1$ equation with two unknowns, and therefore three circles ($n = 3$) are required to derive a unique solution. In practice, the pseudo-ranging is not perfectly estimated, and therefore a condition that three circles are intersect at the same point is considered to be a rare case.

3.2 Centroid of Intersection Polygon Method

Due to uncertainty in ranging, the estimate value can be more or less than the actual one. The position technique in this section simply determines the internal intersect points that are formed into a polygon[2]. For example, Figure 3.2 shows that there are four inner intersection points —$A(x_A, y_A), B(x_B, y_B), C(x_C, y_C), D(x_D, y_D)$.

(a)	(b)
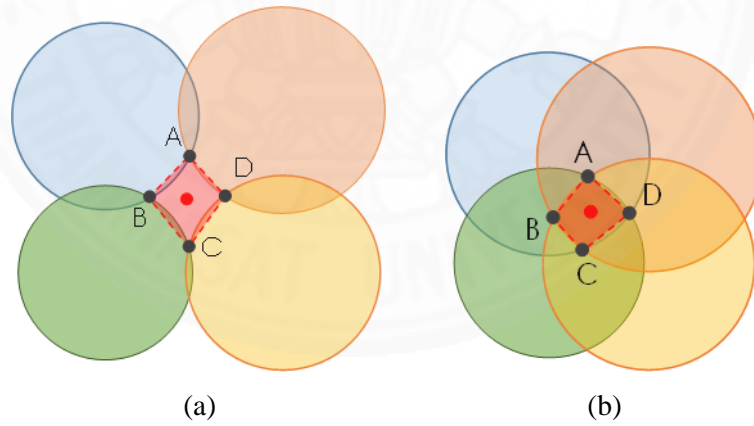
Figure 3.2 Geometric centroid of intersection polygon. (a) Under estimate of ranging. (b) Over estimate of ranging.

This forms a polygon named $ABCD$ and its centroid is an arithmetic averaging of corner coordinates as expressed in (3.8).

$$\text{Centroid} = \left(\frac{x_A + x_B + x_C + x_D}{4}, \frac{y_A + y_B + y_C + y_D}{4} \right) \tag{3.8}$$

8

3.3 Least Square Estimation Method

Least Square Estimation (LSE) method or more specifically Levenberg-Marquardt algorithm [13] is the one of the most widely used algorithms for a positioning determination. The concept of this method is to minimize the summation of error square known as an objective or cost function. The estimation errors are shown in Figure 3.3.
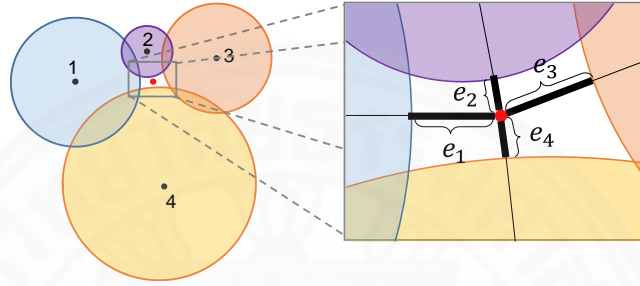
Figure 3.3 Estimation error in pseudo-ranging.

For the positioning determination method[12], the cost function is

$$F(x,y) = \frac{1}{2}\sum_{i=1}^{n} e_i^2 = \frac{1}{2}\sum_{i=1}^{n}(\hat{r}_i - r_i)^2 = \frac{1}{2}\sum_{i=1}^{n} f_i^2(x,y) \qquad (3.9)$$

$$f_i(x,y) = e_i = \hat{r}_i - r_i = \sqrt{(x-x_i)^2 + (y-y_i)^2} - r_i \qquad (3.10)$$

where (x_i, y_i) is a center point, e_i is estimation error, $\hat{r}_i$ and r_i are an exact and measured distance from center point of ith circle, respectively.

Differentiate (3.9) with respect to its independent variables yields

$$\frac{\partial F}{\partial x} = \sum_{i=1}^{n} f_i \frac{\partial f_i}{\partial x}$$

$$\frac{\partial F}{\partial y} = \sum_{i=1}^{n} f_i \frac{\partial f_i}{\partial y} \qquad (3.11)$$

Expand (3.11) and rearrange in a matrix form

9

$$\begin{pmatrix} \frac{\partial F}{\partial x} \\ \frac{\partial F}{\partial y} \end{pmatrix} = \begin{bmatrix} \frac{\partial f_1}{\partial x} & \frac{\partial f_2}{\partial x} & \cdots & \frac{\partial f_n}{\partial x} \\ \frac{\partial f_1}{\partial y} & \frac{\partial f_2}{\partial y} & \cdots & \frac{\partial f_n}{\partial y} \end{bmatrix} \begin{pmatrix} f_1 \\ f_2 \\ \vdots \\ f_n \end{pmatrix} \tag{3.12}$$

$$\mathbf{g} = \mathbf{J}^{\mathrm{T}}\mathbf{f}$$

$$\text{Jacobian matrix, } \mathbf{J} = \begin{bmatrix} \frac{\partial f_1}{\partial x} & \frac{\partial f_1}{\partial y} \\ \frac{\partial f_2}{\partial x} & \frac{\partial f_2}{\partial y} \\ \vdots & \vdots \\ \frac{\partial f_n}{\partial x} & \frac{\partial f_n}{\partial y} \end{bmatrix} \tag{3.13}$$

Practically, the solution for this method is computed in an iterative manner and the governing equation is given below.

$$\mathbf{P}_{k+1} = \mathbf{P}_k - (\mathbf{J}_k^{\mathrm{T}}\mathbf{J}_k)^{-1}\mathbf{J}_k^{\mathrm{T}}\mathbf{f} \tag{3.14}$$

where $\mathbf{P}_k$ is a solution vector at k^{th} iteration.

Both centroid of intersection polygon and LSE methods are used as a trilateration algorithm later in section 6.4.

Chapter 4

Indoor Localization with Bluetooth Low Energy

4.1 Bluetooth Low Energy Technology

Bluetooth Low Energy (Bluetooth LE or BLE), also known as *Bluetooth Smart*, is an additional subset of the *Classic Bluetooth*. It has been introduced as part of the Bluetooth core specifications since version 4.0 in June 2010 by the Bluetooth Special Interest Group (Bluetooth SIG). It aims at sending small amount of data within a short range such as sending sensor values or control commands. BLE shares some similarities with the Classic Bluetooth; however, BLE is not backward compatible.

4.1.1 Frequency Channels

Both BLE and Classic Bluetooth use the same unlicensed Industrial Scientific and Medical (ISM) at 2.4 GHz band, but they divide this frequency band differently, leading to different number of channels. The Classic Bluetooth has 79 channels (1 MHz apart) compared to 40 channels (2 MHz apart) in BLE, and these channels are obviously placed in different spacing. These make them incompatible implying that they cannot communicate with each other. The channel name and its corresponding center frequency in BLE are shown in Figure 4.1.
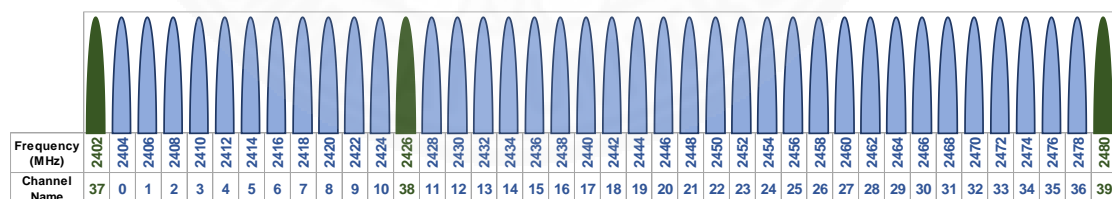
Figure 4.1 Channel names and center frequencies in BLE.

4.1.2 BLE State Machine

BLE has the ability to transfer data with or without making a connection between devices. Channels 37, 38, and 39 called *Advertising Channels* are used only in unconnected device for transferring data. According to Bluetooth Core Specifications [1] for an unconnected device, it can be mostly either *Advertising State* or *Scanning State*. The device in Advertising State periodically advertises or broadcasts a data

11

packet within a pre-defined interval on each Advertising Channel one after the other. The device in Scanning State also periodically scans any incoming advertising packet on each Advertising Channel with larger interval in order to guarantee a reception of a packet from advertiser in a particular channel. Once the scanner received a packet, it can request the other set of advertising packet from an advertiser (if available) or ask for a connection. If the scanner decides to connect, it will enter into *Initiating State* and *Connection State*, subsequently. After establishing the connection, the advertiser will then stop advertising and the data transferring takes place in the remaining 37 channels (Channel 0 to 36) called *Data Channels*. All possible transitions of BLE device are illustrated in Figure 4.2.
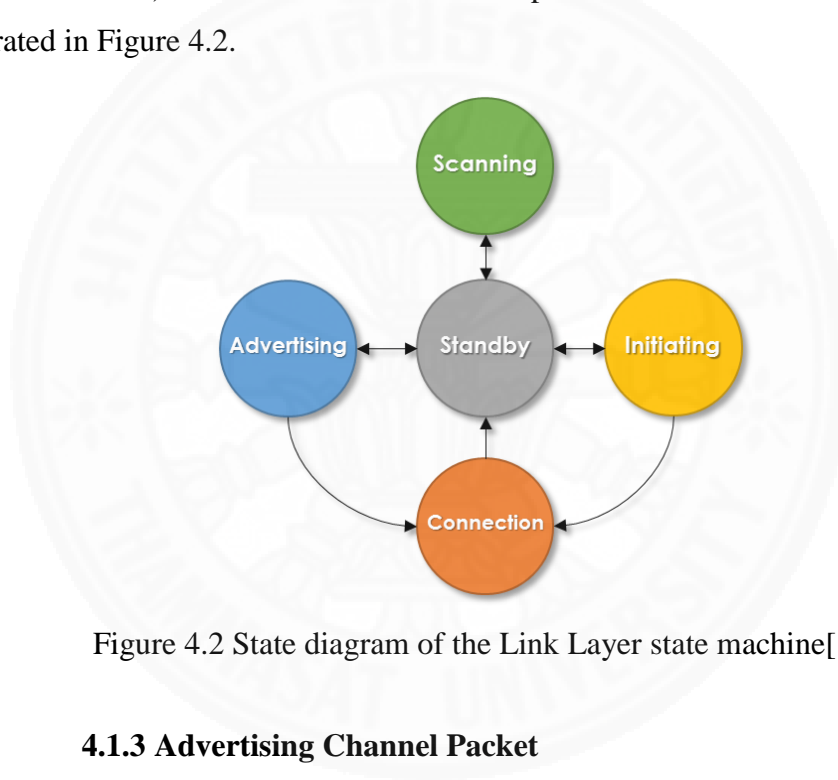
Figure 4.2 State diagram of the Link Layer state machine[1].

4.1.3 Advertising Channel Packet

In Advertising State, the maximum size of data that the advertiser can broadcast is 47 bytes which contain the following fields: *Preamble*, *Access Address*, *Packet Data Unit (PDU)* and *Cyclic Redundancy Check (CRC)* as shown in Figure 4.3. The Preamble is one byte long used for synchronization at the receiver. It will always be **0xAA** and the Access Address is also a fixed value to **0x8E89BED6**.

12
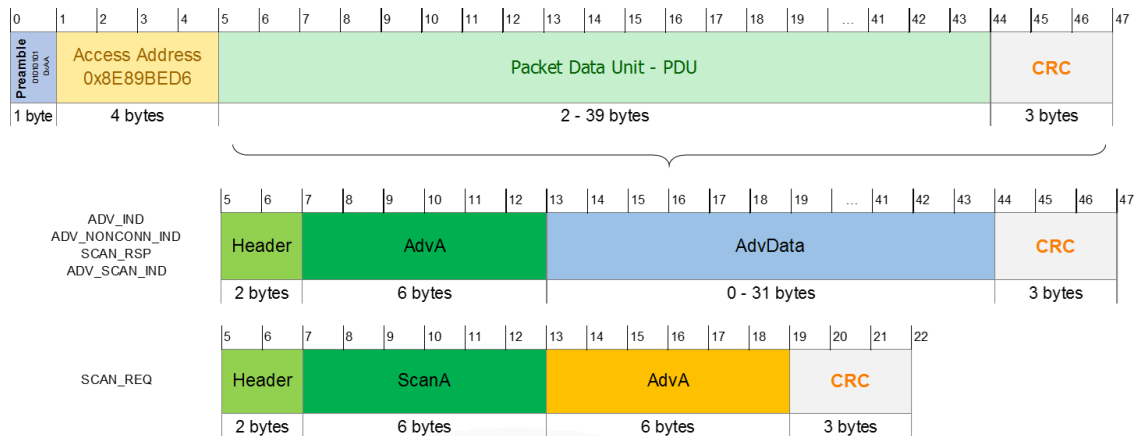
Figure 4.3 Advertising State packet structure.

The PDU consists of header and payload. The header describes the PDU type, length of payload and address type of advertiser and initiator as shown in Figure 4.4. The payload consists of information regarding to its PDU type and length depending on advertising data embedded.
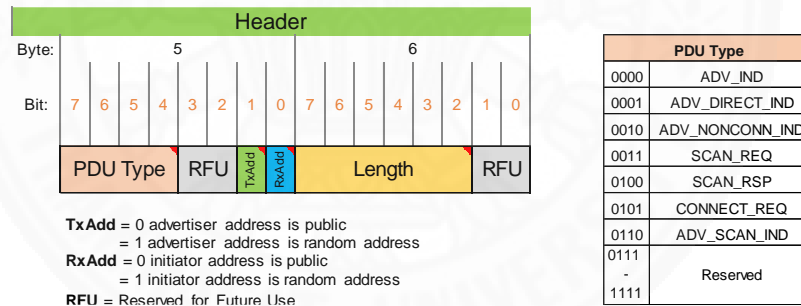
Figure 4.4 Packet Header and PDU Types.

For advertising applications, there are three different PDU types: **ADV_IND** (connectable undirected advertising event), **ADV_NONCONN_IND** (non-connectable undirected advertising event) and **ADV_SCAN_IND** (non-connectable broadcaster with additional information by scan response). The last part of the transmitted packet is the CRC. It is an error-detecting code calculated from the whole packet excluding the preamble field. It uses to validate the packet for possible bit errors. This ensures data integrity for all transmitted packets over the air. For Connection State, a packet frame is different and beyond the scope of this research thesis. This research will focus only on the Advertising State.

13

4.2 Pseudo-Ranging From Bluetooth Low Energy Beacons

Scanner scans for advertising Packet Data Unit (PDU) broadcasted by the advertiser. A single PDU limits data up to 39 bytes. However, the scanner can request for one more PDU by sending SCAN_REQ packet, the advertiser will then response by sending SCAN_RSP packet back. The advertiser is required to advertise the PDU type as ADV_IND or ADV_SCAN_IND in order to inform the scanner that it can response to SCAN_REQ packet.

This research work considers the travel time of a BLE beacon packet after sending to the device and waiting for the corresponding response beacon. The communication protocol has already been established in the Bluetooth Core Specifications [1], which means any device conforming to the specifications can be used as a ranging device given that it needs to calibrate priori. Since there is no special hardware or protocol required, this leads to an ease of implementation.

Multipath interference may occur during receiving the incoming beacon. It will degrade the signal quality while demodulating within the physical layer (PHY) of BLE stack. This may cause bit error in the packet, which in turn results in a bad Cyclic Redundancy Check (CRC) checksum. In this research work, only good BLE packets received at Link-Layer level have been considered by verifying a valid CRC checksum associated with the packet. If not, the packet will be discarded.

4.2.1 Pseudo-Ranging Scheme

In this research work, the capability of scannable advertiser has been utilized to measure a travel time of SCAN_REQ and SCAN_RSP packet. Firstly, the scanner scans for ADV_IND or ADV_SCAN_IND packets and then sends SCAN_REQ to a target advertiser. Immediately after sending SCAN_REQ, the scanner starts a timer. The SCAN_REQ packet is subsequently traveled to the advertiser. As soon as the advertiser received SCAN_REQ packet, it responses back a SCAN_RSP packet with an empty payload to the scanner. Once the scanner received SCAN_RSP packet, it stops the timer. The total RTT is measured in term of CPU clock cycles, which can be converted to an actual travel time if the CPU clock frequency is known. The timing diagram for measuring the RTT is shown in Figure 4.5.

14
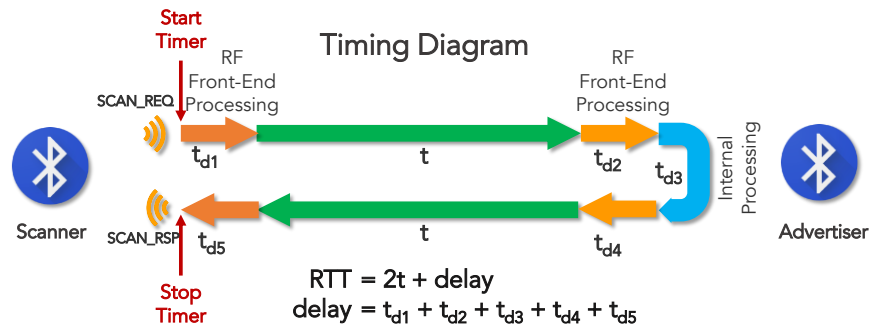
Figure 4.5 Timing diagram of RTT determination by sending SCAN_REQ and receiving SCAN_RSP packet.

4.2.2 Hardware Consideration

In modern BLE modules, they are built based on System on Chip (SoC) microcontroller. It can be programmed to any general purpose software like other microcontrollers. Most of them are based on ARM Cortex-M Series. An nRF5122 from Nordic Semiconductor [14] is one of widely used BLE modules. It is an ultra-low power 2.4 GHz wireless SoC based on a 32 bit ARM-Cortex M0 CPU running at 16 MHz that supports the 2.4 GHz multiprotocol including BLE. According to product specifications [15], the radio tasks are operated by RADIO peripheral block that can be controlled by CPU or other peripherals through Programmable Peripheral Interconnect (PPI). The PPI system enables one peripheral to directly activate other peripherals without waking up the CPU. For instance, the RADIO peripheral can start or stop the TIMER peripheral while the CPU is sleeping. The block diagram of this feature is illustrated in Figure 4.6
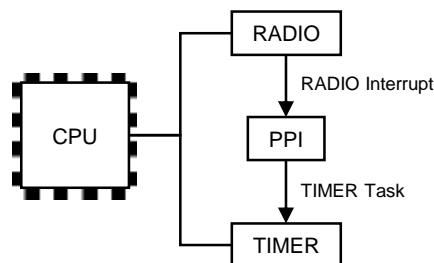
Figure 4.6 Block diagram of PPI to manage RADIO interrupt and TIMER task

15

The RADIO peripheral in nRF51822 allows user to access into a low-level state machine [16] as shown in Figure 4.7. It can be assigned to bypass from one state to another state without a command activation in order to reduce an operating time. It also provides many interrupt events in almost all states as highlighted.
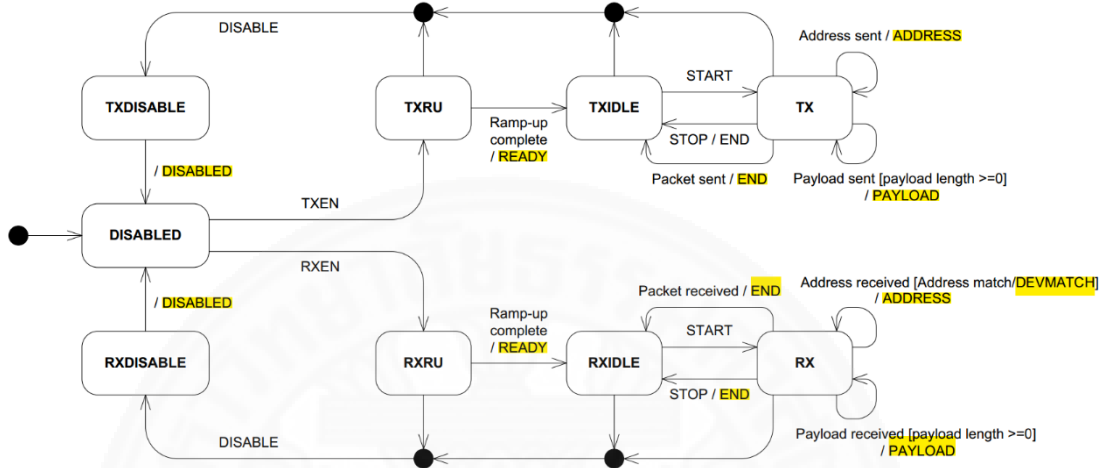
Figure 4.7 Radio state diagram.

The radio transmission and reception sequence for RTT measurement in this work is shown in Figure 4.8. The PPI links END interrupt of the transmitting state to start TIMER task and the DEVMATCH state to stop TIMER. In addition, the END Interrupt Service Routine (ISR) of the receiving state is used to check for CRC validation.
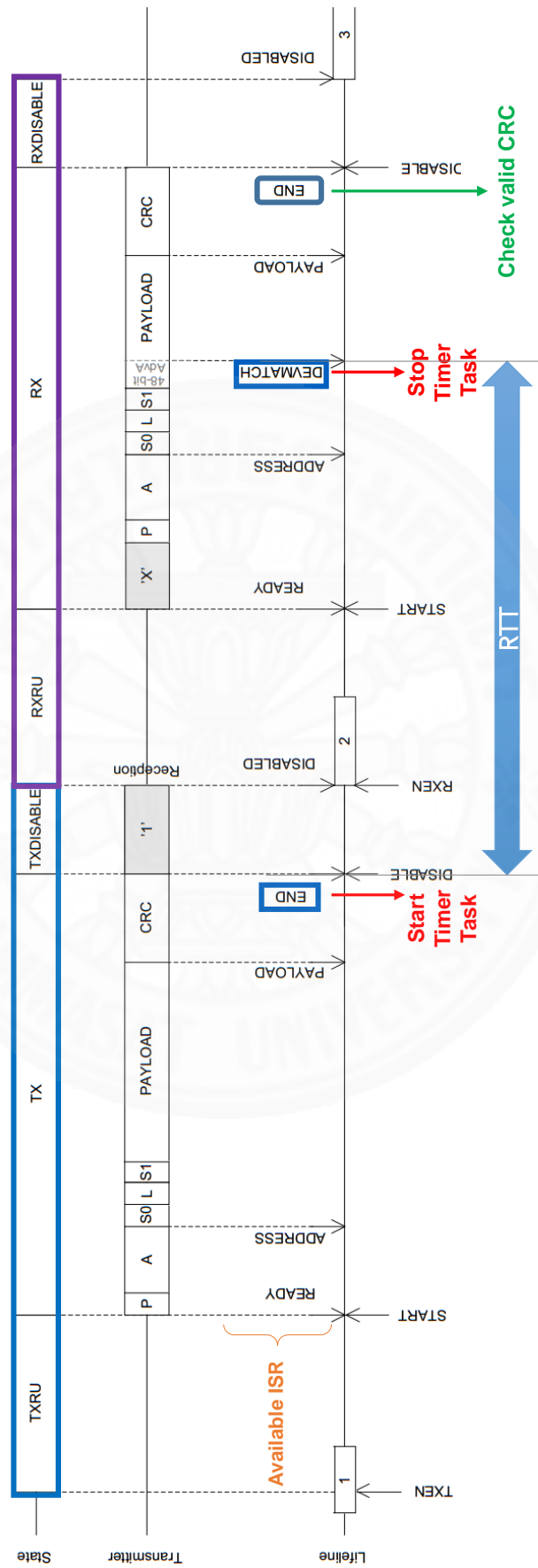
Figure 4.8 Radio transmission and reception sequence for RTT measurement.

17

4.2.3 Delay Time

The delay time is commonly encountered in the RTT ranging approach. This delay comes from an internal processing of both scanner and advertiser. It can adversely reduce the accuracy in ToF-based ranging. Nonetheless, the PPI system in nRF5122 can help reducing the delay since the RADIO peripheral can start TIMER peripheral directly through an internal interrupt without waking up the CPU. One of the reasons that causes an uncertainty of the delay is a clock drift in the clock source, i.e. a crystal oscillator.

4.2.4 Implementation

In this research, a firmware has been implemented to perform specific tasks for measuring the RTT in nRF51822. The firmware was programmed in a bear-metal programming fashion without a full-fledged vendor library called SoftDevice [17]. Hence, the implemented firmware includes only necessary tasks for the RTT measurement.

There are generally two antenna flavors available in BLE module, which are on-board antenna and external antenna. The omnidirectional external antenna is provided in this thesis in addition to an on-board antenna of nRF51822 module in order to make a rotational invariance.

Since the RTT is measured by using the CPU clock, it is necessary to have a high accuracy oscillator. The external Temperature Compensated Crystal Oscillator (TCXO) is considered in this research for reducing the uncertainty of clock drift. The TCXO specification is provided in Appendix A. Figure 4.9 shows the hardware implemented in this research.
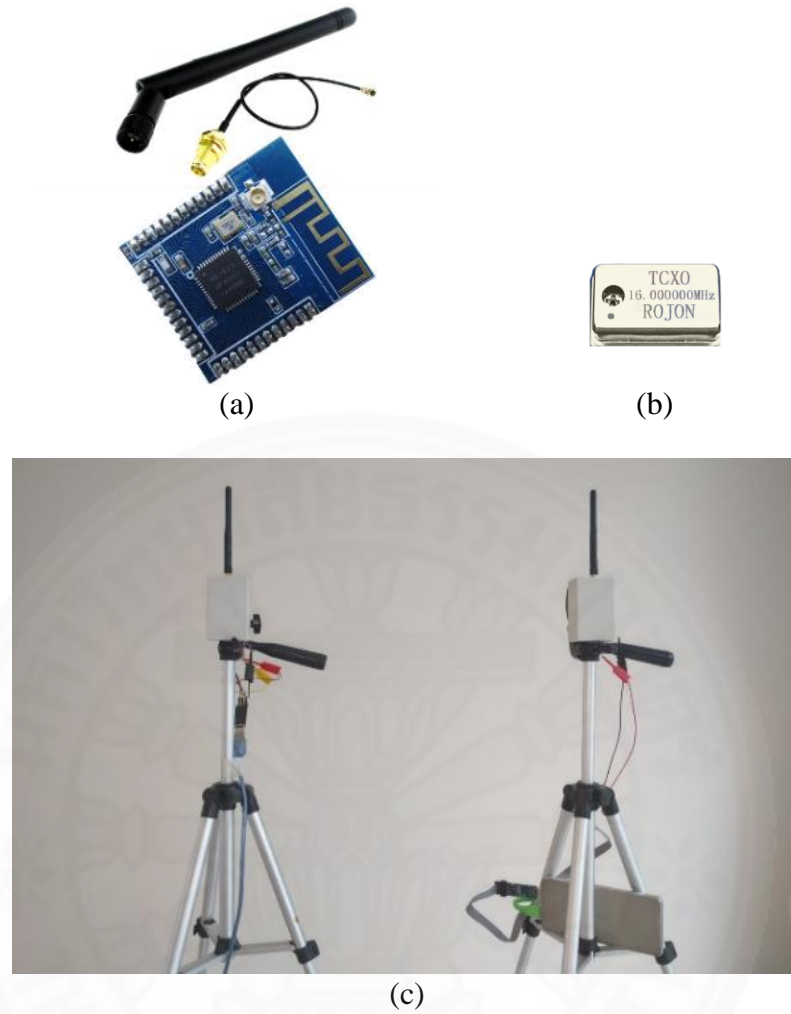
Figure 4.9 Hardware implementation. (a) An nRF51822 module with Omni directional antenna. (b) A Temperature Compensated Crystal Oscillator (TCXO). (c) BLE scanner (left) and BLE advertiser (right).

4.3 Kalman Filter

The radio frequency, by its nature, is subjected to noise. To measure RTT using radio wave is inevitable to encounter with the noise. This is why Kalman filter is taken into account. It has be applied to many applications [18]. The Kalman filter is an estimator of variables in noisy measurements. It consists of prediction and correction processes. These processes are in a recursive manner as they take the history of measurements into account. The one-dimensional linear model Kalman filter is considered in this thesis. This means the state transition from the current state to the next state is a linear transformation.

19

The general form of the transition model is shown as follows[19]:

$$x_t = A_t x_{t-1} + B_t u_t + \varepsilon_t \qquad (4.1)$$

where x_t is the current state that is calculated from a combination of the previous state x_{t-1}. A_t is a state transition matrix, B_t is a control-input matrix, u_t is a control value, and ε_t is a process noise. For RTT measurement, it is assumed that a device does not move for a short interval. In other words, the RTT is expected to be a constant over time such that the model ignores u_t and A_t is an identity matrix.

Hence,

$$x_t = x_{t-1} + \varepsilon_t \qquad (4.2)$$

The other part of Kalman filter is the observation model:

$$z_t = C_t x_{t-1} + D_t u_t + \delta_t \qquad (4.3)$$

where z_t is a measurement value, C_t is a transformation matrix and δ_t is a measurement noise. Since RTT is measured directly and there is no input value, the above equation is reduced to

$$z_t = x_{t-1} + \delta_t \qquad (4.4)$$

The transition and observation models, respectively, have already been prepared as shown in (4.2) and (4.4). There are two sets of equations in prediction and correction processes of Kalman filter. The next step is to determine the necessary parameters and initial values, and then iterates them recursively as illustrated in Figure 4.10.

20

Prediction

1.Predict next value
$$x_t^- = x_{t-1}$$
2.Predict next error covarience
$$P_t^- = P_{t-1} + Q$$

Start: $t = 0$

Correction

1.Compute Kalman Gain
$$K_t = \frac{P_t^-}{P_t^- + R}$$

2.Update estimate with z_t
$$x_t = x_t^- + K_t(z_t - x_t^-)$$

3.Update error covarience
$$P_t = (1 - K_t)P_t^-$$

$$t = t + 1$$
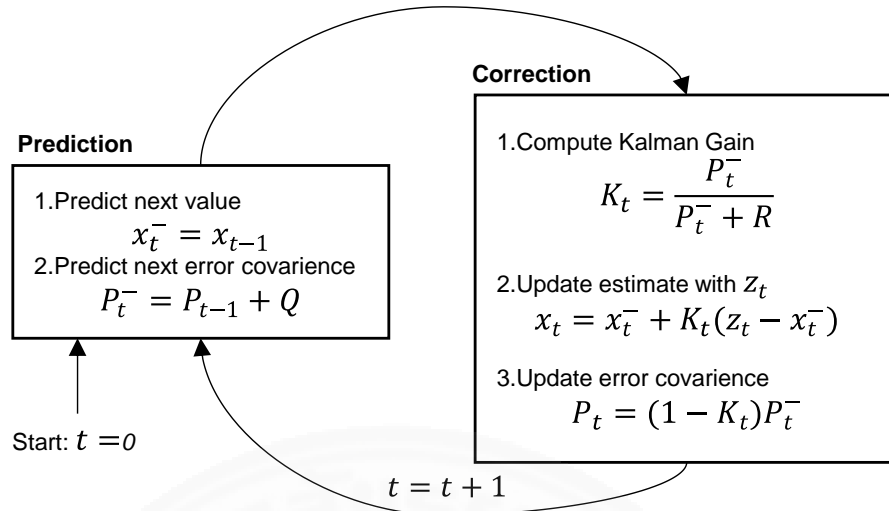
Figure 4.10 Kalman filter iteration flow[19].

The remaining parameters to be determined are the process noise (R) and the measurement noise (Q).

In summary, this chapter describes the indoor localization with BLE and relevant factors associated with the hardware implementation, which will be utilized to obtain experimental results later on.

21

Chapter 5
Real-Time Tracking System

5.1 Inverse Positioning Method

Typically, the estimate position is calculated directly in a mobile unit called *direct positioning method*. This means the mobile unit has to scan the advertising beacon from known locations, and then performs a calculation for pseudo-ranging and final position subsequently. The mobile unit is required to be a device that is powerfully enough such as smartphone to perform this task. In this thesis, the *inverse positioning method* has been utilized, and the system architecture is illustrated in Figure 5.1. The pseudo-ranging is determined by anchor nodes located at predefined locations. The anchor nodes consist of BLE module used for ranging and Wi-Fi module used for transferring data. The estimated pseudo-ranging is then sent from the anchor nodes to a back-end server where the final position is evaluated. The server provides several services to manipulate incoming data. The mobile unit in this system, named tag, is no longer required to be a smart device, and thus even a simple and low-cost BLE tag can be used. However, the use of a simple BLE tag comes at a cost of the back-end server.
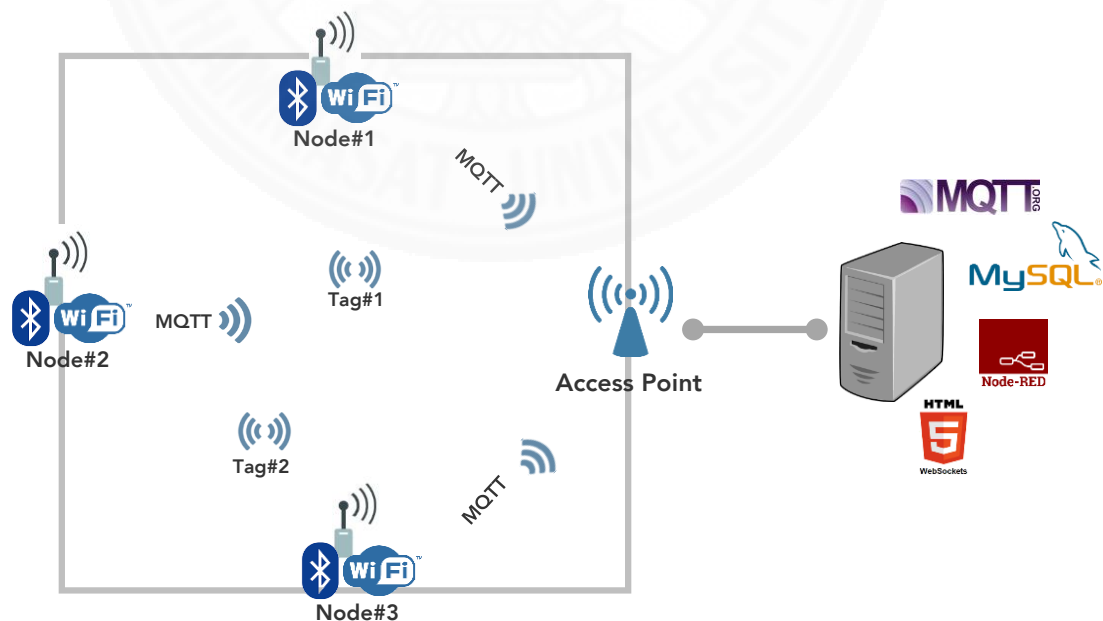
Figure 5.1 System architecture for real-time positioning system.

The flow diagram in Figure 5.2 demonstrates the proposed real-time tracking system in this thesis. There are two separated processes, data acquisition and trilateration, which operate concurrently.

(a)   (b)
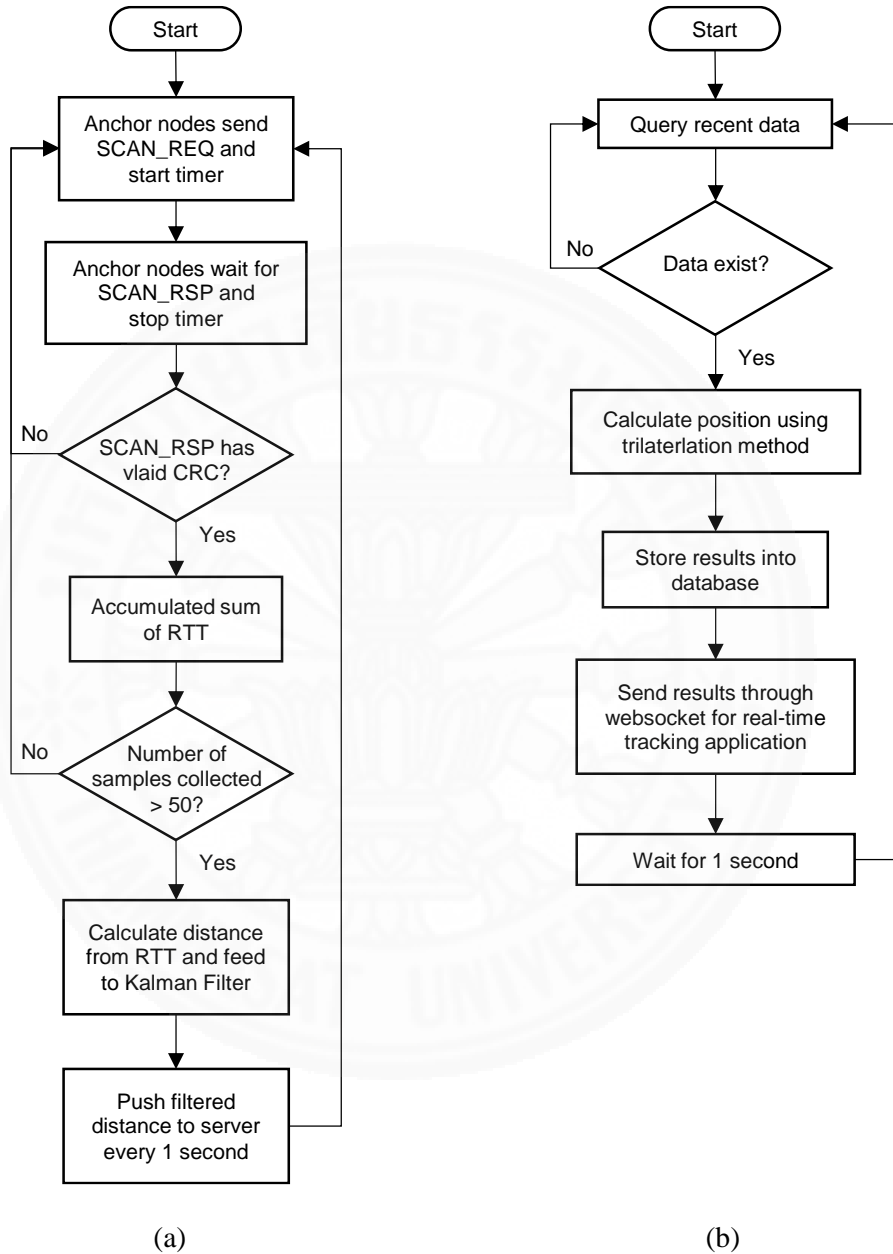
Figure 5.2 Flow charts of the real-time tracking system. (a) Data acquisition flow (b) Trilateration flow.

5.2 Services on Server

According to Figure 5.1, it can be seen that there are several technologies being employed to build up a real-time tracking system using the inverse positioning

23

method. These services consist of real-time messaging, database, data processing and web services. The real-time messaging service is used for sending pseudo-ranging data from the anchor node to the server, and then storing in database. The data processing service then periodically query the recent data from database in order to calculate and store positions if available into the database. Additionally, this service also provides a websocket server in order to send positions immediately after the calculation to a web front-end for real-time application. All these services are elaborated in following sections.

5.2.1 Message Queue

Message Queue Telemetry Transport (MQTT)[1] is a lightweight client-server based messaging protocol with a minimal protocol overhead. It is publish/subscribe scheme as shown in Figure 5.3, which requires a central broker aimed at Machine to Machine (M2M) that has constrained environments. The sender called **publisher** sends data associated with topics directly to the broker without having to know who the recipient is. The receiver called **subscriber** requests for the data from the broker by subscribing the interesting topics to the broker.

Figure 5.3 MQTT Publish/Subscribe scheme.

---

[1] http://mqtt.org

24

The main operation of the broker is looking for the topics from the publishers, and then redirecting these messages to all subscribers that request the same topic accordingly.
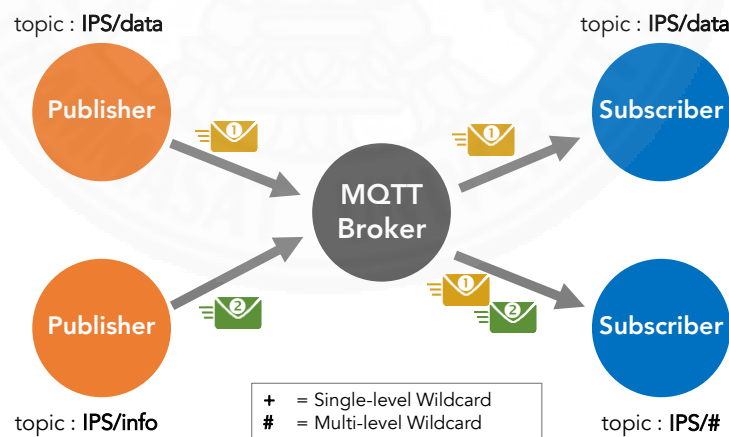
In order to receive messages for different topics having a similar structure at once, MQTT also provides topic wildcards for the subscriber to subscribe to the broker. The meaning and examples are shown in Table 5.1.

Table 5.1 MQTT topic wildcards

Symbol	Meaning	Examples
+	A single level wildcard that matches one topic level. It can be used more than once in a topic.	IPS/+/node IPS/data/+
#	A multiple level wildcard that matches any number of levels and must be the last character in a topic.	IPS/# IPS/data/#

Topics and example messages used in the thesis are listed as follows:

- **IPS/data**: for sending estimated distances of each tag scanned from the particular anchor node. For example, the anchor node **IPS001** found three tags having ID **1**, **2** and **3** at distance 1.23, 4.23 and 5.3 meters, respectively. Therefore, the message becomes:

  ```
  IPS001:1,1.23;2,4.23;3,5.3
  ```

- **IPS/info**: for sending current configurations of the anchor node. It consists of anchor ID, its coordinates and interval (millisecond) for sending data to the broker. An example message subjected to this topic is:

  ```
  IPS001, 0.0, 2.5, 0.0, 1000
  ```

- **IPS/***node_id* : for sending a command to change configurations of the specified anchor node. For example, to change the anchor node **IPS001**, the MQTT topic will be **IPS/ IPS001**. An example message subjected to this topic is:

  ```
  { "X" : 1.23, "Y" : 4.567, "Z" : 0.0, "interval" : 1000 }
  ```

- **IPS/lwt**: for the broker to notify which the anchor node is not response.

25

5.2.2 Database

In the inverse positioning method, it utilizes MySQL[2] as a database service. Four tables are implemented to store all the data provided by the anchor nodes that sent through the MQTT broker along with the positioning results after the calculation. These tables are:

- **tag**: storing tag ID and properties such as name and description.

- **node**: storing node ID, coordinates, sending interval, description and its status.

- **tag_distance**: storing scanned results from anchor node. This is intermediate data used for the positioning calculation. Since this is the real-time system, these data are deleted after the position is obtained.

- **position**: storing the final position after the calculation.

The database schema, relations and sample dataset are illustrated in Figure 5.4.
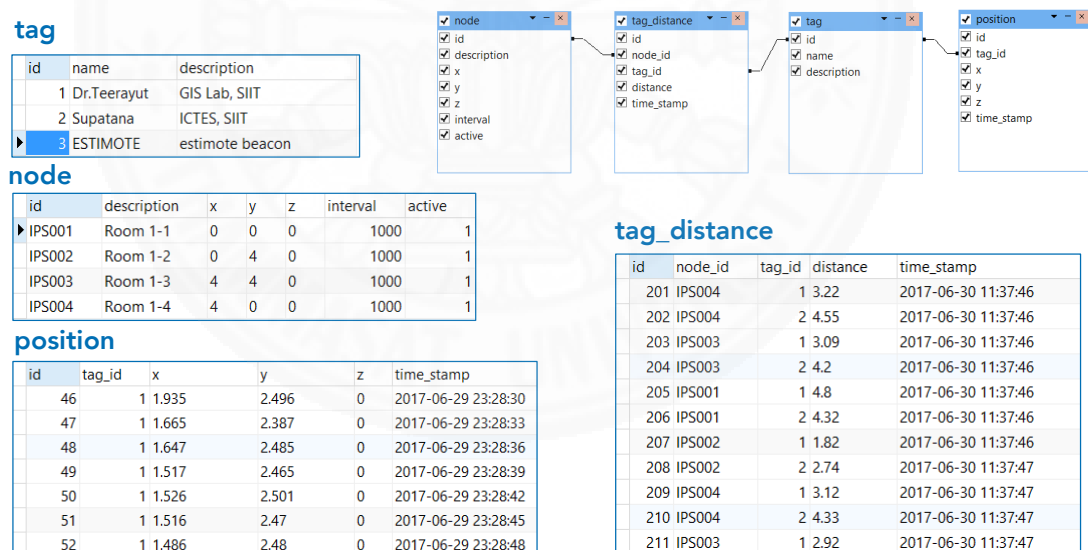
Figure 5.4 Database schema, relations and sample dataset.

26

5.2.3 Data Processing

This is the main part of the real-time tracking system. It connects all services, i.e. MQTT broker, websocket and MySQL, altogether. Moreover, it handles all the incoming data by forwarding them to relevant services, and performs the trilateration. All these tasks are implemented in Node.js[3] or more specifically Node-RED[4]. Node.js is a server-side JavaScript language based on V8 JavaScript engine. Node.js uses an event-driven, non-blocking I/O model that makes it lightweight and efficient especially in real-time application. Node-RED is a flow-based programming diagram based on Node.js. It provides a browser-based editor for programming by placing programming blocks that perform a specific task, and then wiring them together as shown in Figure 5.5. Custom block can also be implemented in addition to default ones. Trilateration block has been implemented in this thesis for the positioning determination.
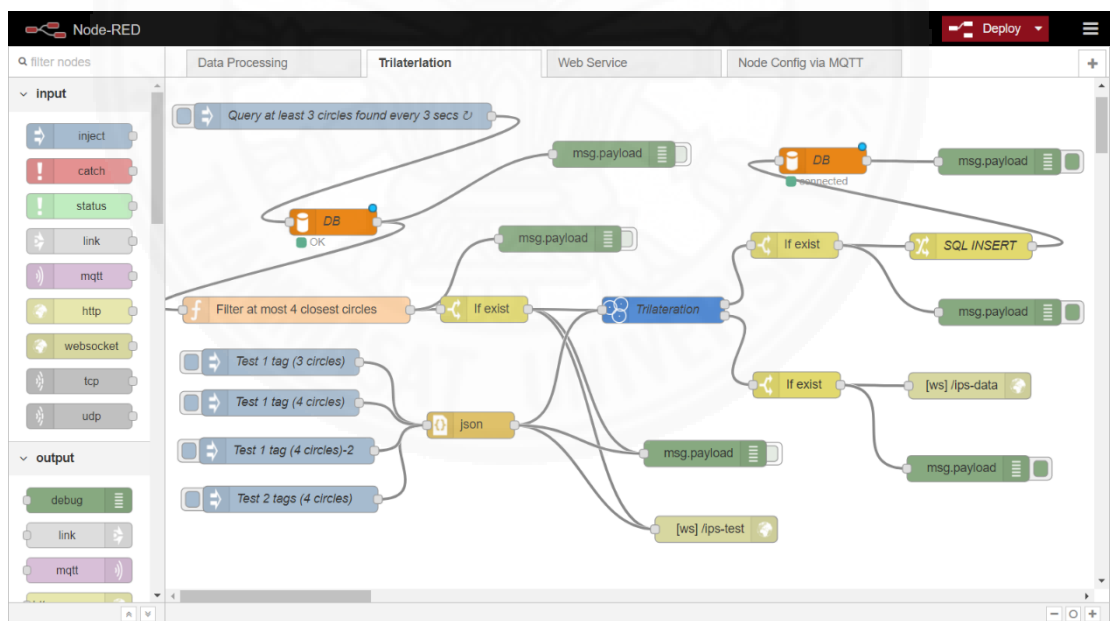
Figure 5.5 Data processing by Node-RED

---

[3] https://nodejs.org

[4] https://nodered.org

27

5.2.4 Front-end Web Application

According to Figure 5.5, the resulting position will be sent to two channels immediately after performing the trilateration. One is sent to store in database and the other is sent through websocket. A front-end web application opens this socket for the incoming data pushed by the server, and therefore it can show the position in real-time. A simple front-end web application is shown in Figure 5.6
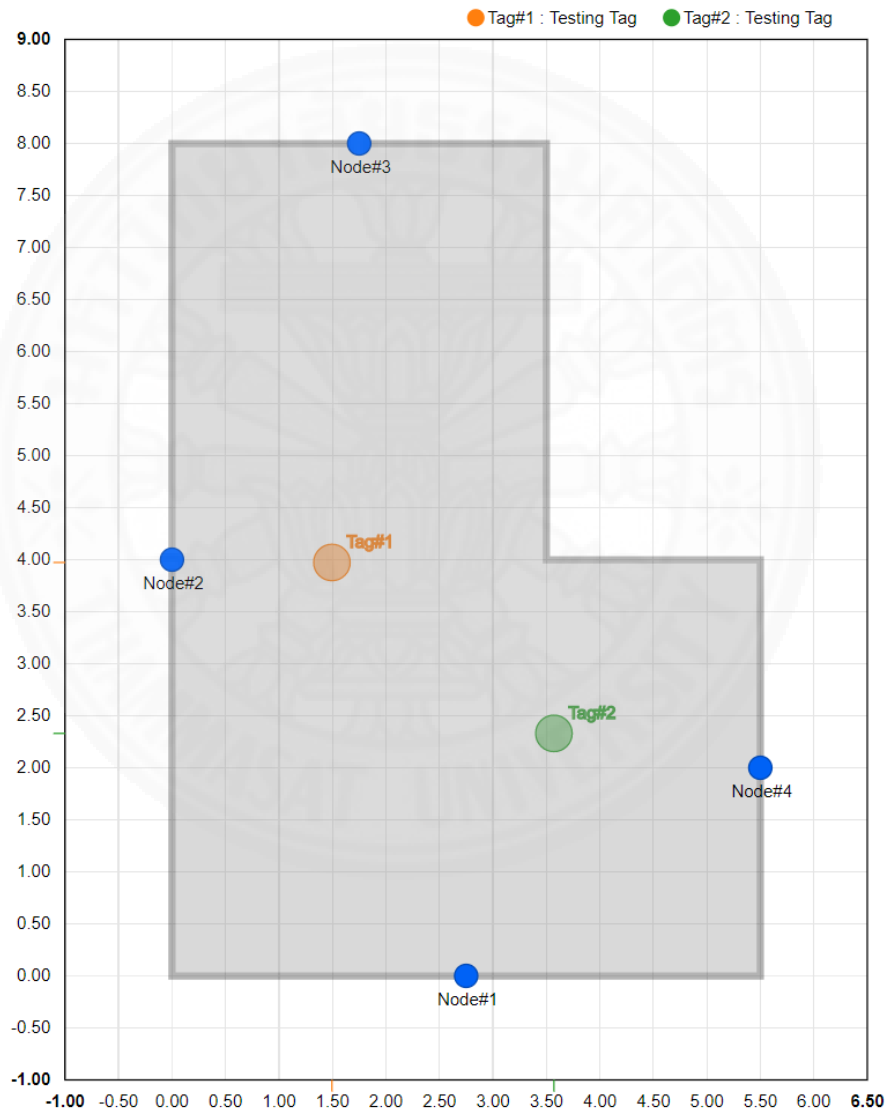
Figure 5.6 Front-end web application.

The next chapter will present the experiments and results obtained using the real-time tracking system described in this chapter.

28

Chapter 6
Experiments and Results

Experiments in this thesis are divided into four sections. The first part is a pseudo-ranging test between two nodes based on RTT of BLE beacon to find parameters that represent a relationship between RTT and distance. The second section is a study on data throughput among four anchor nodes and a tag to observe packet collision problem while all nodes concurrently send and receive packets. Kalman filter test in the third section is also investigated for smoothing out measured data. The last section utilizes the same technique as in the first section to find a distance between tag and four anchor nodes located at each side of a testing room, and then the estimated location of tag is calculated by the trilateration method.

6.1 Pseudo-Ranging Test

Regarding to a proof of concept for the RTT ranging using a low-cost device, it needs to minimize unknown factors. Therefore, the experimentation is conducted in a line-of-sight area. The experimentation setup is shown in Figure 6.1. This RTT measurement method in this work can be applied to not only indoor but also and outdoor area. For longer testing space, the test in this section was done outdoor with surrounding masonry walls.

Testing distance between the advertiser and the scanner is conducted for one meter apart at a time ranging from 1 meter up to 10 meters apart. For each observed distance, there are three advertising channels being considered and 5,000 samples were collected for each advertising channel, i.e. 15,000 samples in total. Sample rate used in the study is approximately 20 samples/sec. The RTT and RSSI are collected at each sample.

Figure 6.1 Experimentation setup.

The probability distributions of CPU cycle counts while measuring the RTT of each advertising channel are illustrated in Figure 6.2. The three advertising channels are designated as Channels 37, 38 and 39. The testing distances at 2.0m, 4.0m, 6.0m and 8.0m are presented in Figure 6.2(a) to (d), respectively.

(a)

(b)

(c)

(d)

30
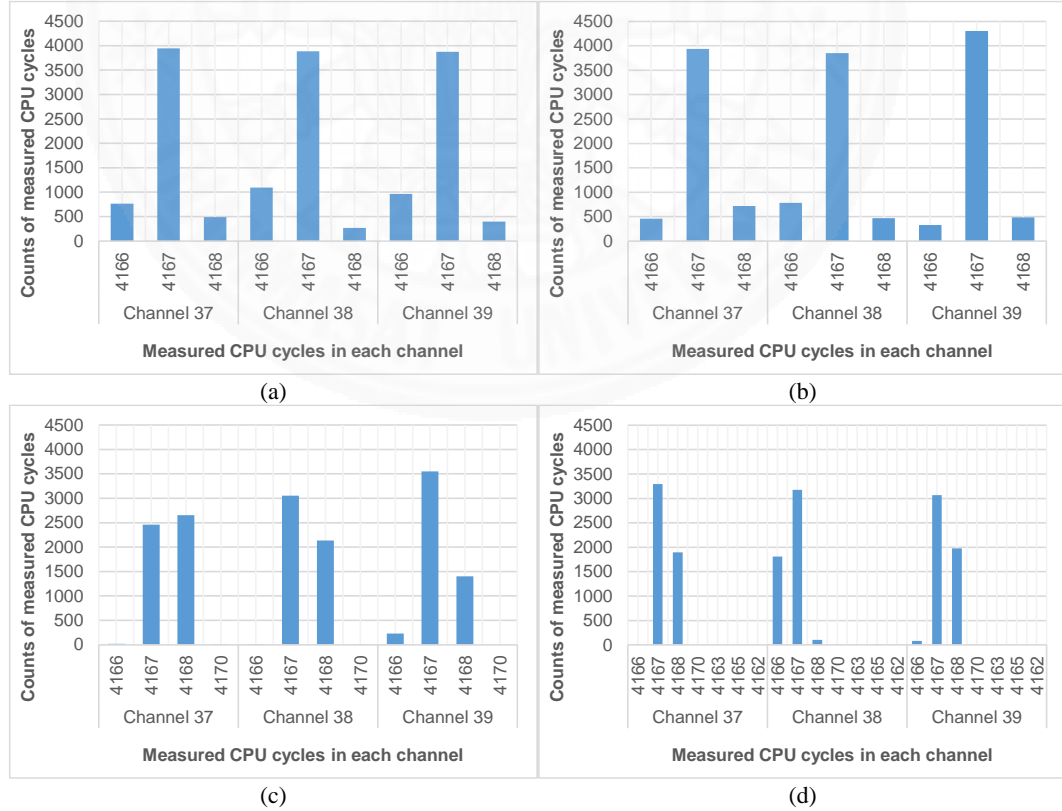
Figure 6.2 Distributions of CPU cycle counts in each advertising channel. (a) Data collected at 2.0 m. (b) Data collected at 4.0 m. (b) Data collected at 6.0 m. (b) Data collected at 8.0 m.

The CPU cycle counts can be converted to the actual RTT by multiplying the period of CPU clock that is 1/16 μs. The relationships between the average RTT and the distance of each advertising channel are plotted and shown in Figure 6.3. It can be seen that the relationships are relatively different among the three channels. Channel 39 tends to exhibit the best linearity.
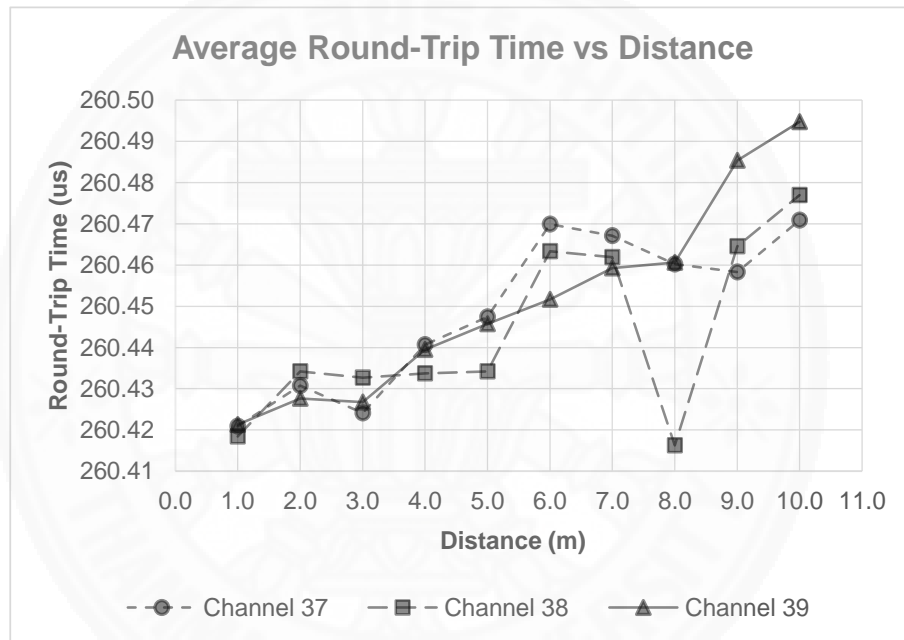
Figure 6.3 Relationship between the average RTT and the distance.

Moreover, it has been observed that the RSSI exhibits a periodic pattern as shown in Figure 6.4(a). This is because the scanner periodically scans in Channels 37, 38 and 39. The distribution of the RSSI of all samples in each channel is also shown in Figure 6.4(b).

31
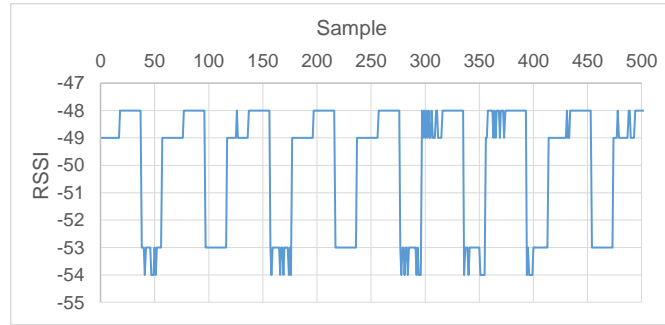
(a)
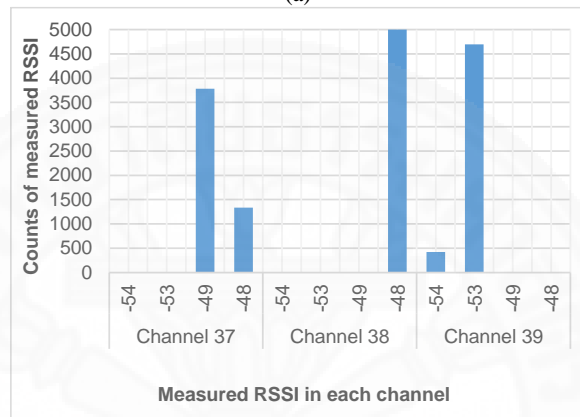
(b)

Figure 6.4 RSSI samples at distance 4.0 m. (a) The first 500 RSSI samples. (b) Distribution of RSSI in each advertising channel.

Figure 6.5 shows that the sensitivity in each channel varies along the distance. For example, the best RSSI at distance 3.0m is from Channel 38, whereas the best RSSI at 8.0m is from Channel 37.

32
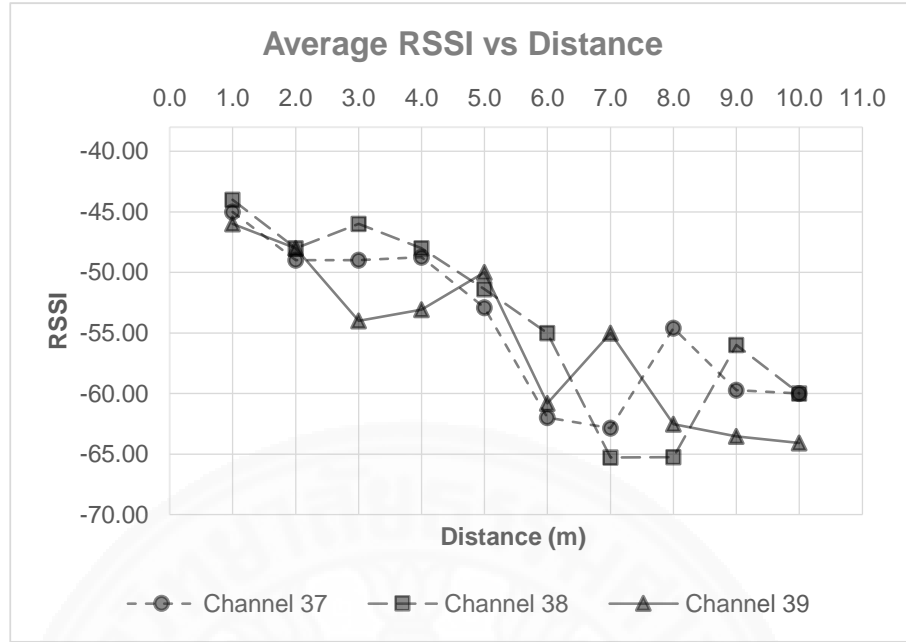
Figure 6.5 Average RSSI vs. Distance.

Finally, the equation to represent the relationship between the RTT and the distance has been developed. This relationship is applied to the specified hardware only. In other words, another experimentation will be required for determining an applicable relationship equation when utilizing a different hardware. The equation can be obtained by applying the linear regression to the average RTT of all channels shown in Figure 6.6 in order to determine parameters as derived in (6.1).

$$RTT = 0.0061 \cdot distance + 260.41; \ R^2 = 0.8519 \qquad (6.1)$$

Alternatively, by considering Figure 6.3 in conjunction with Figure 6.5, the channel offering the best RSSI can be selected and used to derive the relationship of the RTT and the distance as expressed in (6.2) and shown in Figure 6.6. This alternative equation will improve the results as verified by the coefficient of determination, R^2. Thus, equation (6.2) has been used for estimating the distance once the RTT of the BLE packet is known.

$$RTT = 0.0056 \cdot distance + 260.42; \ R^2 = 0.9033 \qquad (6.2)$$
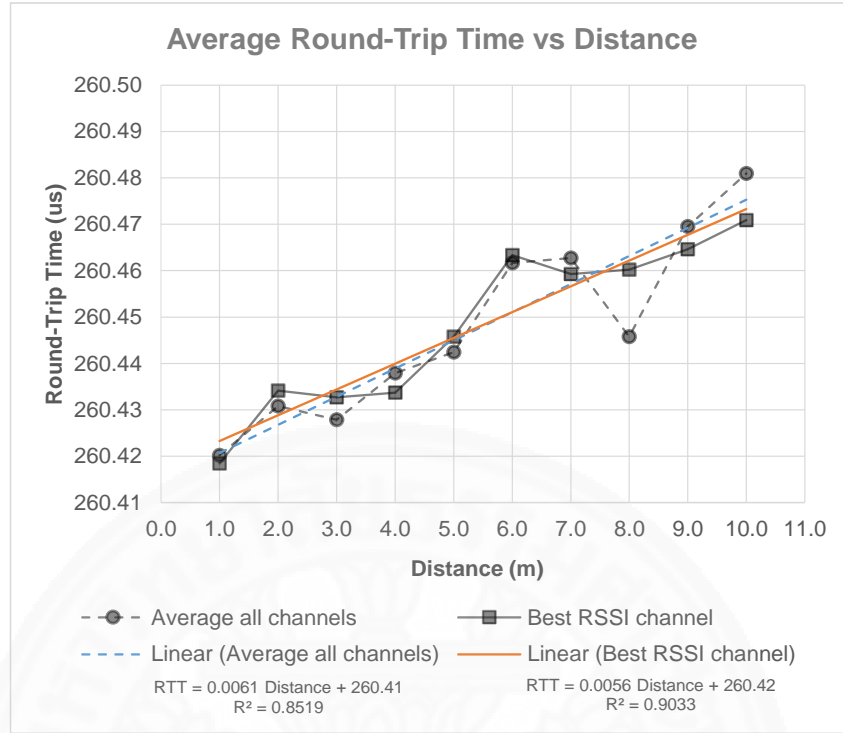
Figure 6.6 Representation relation of RTT and distance.

6.2 Packet Response Rate Test

Pseudo-ranging by RTT with a low frequency clock (16 MHz in this thesis) requires a sufficiently large number of samples in order to obtain a statistically meaningful average value. In section 6.1, there are only two devices acting as the anchor node and the tag in the positioning system, and therefore the problem in the packet collision does not occur. However, the actual positioning system contains multiple anchor nodes and the targeted tag that has to response to multiple requests from these anchor nodes. Each anchor node has to collect as much data as possible by sending SCAN_REQ to the tag. This leads to the congestion or sometime collision of SCAN_REQ packets in the targeted tag so as to serve a large amount of requests from all anchor nodes. Normally, a tag broadcasts an advertising packet (ADV_IND or ADV_SCAN_IND). Each anchor nodes will then send SCAN_REQ immediately after receiving the advertising packet. In this thesis, the broadcasting step is ignored in order to increase the response rate. The pseudo-ranging begins with all anchor nodes sending their own SCAN_REQ simultaneously to the targeted tag. The targeted tag then sends

34

SCAN_RSP back to a particular anchor node corresponding to the packet that can be captured.

The data throughput depends on the advertising interval of the advertiser, the scanning interval and the number of the scanners, and the size of the packet. Obviously, the smaller interval value can increase the data rate. However, it needs to provide a processing time and frame spacing for sending and receiving a packet or any other calculation such as filtering data, otherwise the device will crash or malfunction. The channel hopping interval of both tag and anchor node shown in Figure 6.7 are firstly assigned to 30ms and 5ms, respectively. This will ensure that the packets can reach the targeted tag where the channel of both devices is the same. The tag will keep scanning and responding all the time one after another within the channel hopping interval, whereas the anchor node will send only a single request and then wait for an incoming response at the very beginning of the interval.

Tag : Scanning SCAN_REQ/ Reply SCAN_RSP			
Channel	CH37	CH38	CH39	so on…
time (ms)	30	30	30	

(a)

Anchor node : Sending SCAN_REQ/ Receiving SCAN_RSP																		
Channel	CH37	CH38	CH39	CH37	CH38	CH39	CH37	CH38	CH39	CH37	CH38	CH39	CH37	CH38	CH39	CH37	CH38	CH39	so on…
time (ms)	5	5	5	5	5	5	5	5	5	5	5	5	5	5	5	5	5	5	

(b)

Figure 6.7 Interval for channel hopping of a tag and anchor nodes. (a) A tag listens for SCAN_REQ and replies SCAN_RSP. (b) Anchor node sends SCAN_REQ and receives SCAN_RSP.

To investigate the response rate of data acquisition, a tag was placed 1.5 m and 3.0 m apart from four anchor nodes, shown in Figure 6.8, while letting all the four anchor nodes to send SCAN_REQ simultaneously. At the 1.5m distance, the test was done twice for comparison purposes.
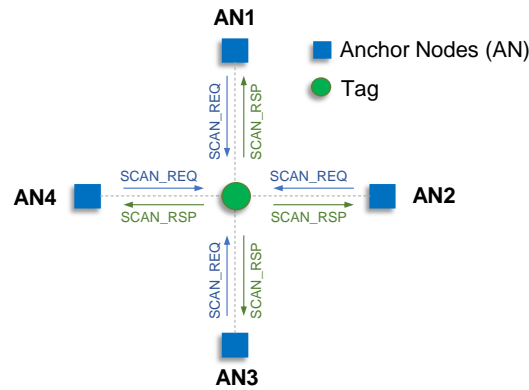
Figure 6.8 Device setup for packet response rate test.

The requested packet successfully received by a tag was monitored for 5 minutes while the MAC address of the anchor node corresponding to that request was also recorded. The response rate is determined from the number of packets divided by the elapsed time. The recorded data are summarized and shown in Table 6.1.

Table 6.1 Packet response rate.

Anchor Node ID	Response Rate (samples/sec)		
	1.5m (Trial 1)	1.5m (Trial 2)	3.0m
1	49.88	52.13	49.45
2	49.51	32.81	46.60
3	45.45	36.96	36.89
4	50.57	47.13	47.03
Total	195.40	169.04	179.97

The results show that the rate of each anchor node for receiving SCAN_RSP is uneven, variable and independent of distance. For example, the total response rate at 1.5m of both trials are different. Anchor node 1 in the second trial has an increase rate whereas the rest of the rates are decreased. The distance and total response rate are also uncorrelated which can be seen from the results of the 3.0m distance compared to both 1.5m trials. The major reason that causes a variation in the response rate is the packet collision. Since the anchor nodes send out the SCAN_REQ with the same interval at every 5 ms or 5000 μs. The worst case occurs when all anchor nodes start up at the same time. They all send packet out at the same time with the same channel. This leads to a high possibility of interference. The other experiment on packet response rate was conducted in the same way as the previous one, but the interval for

36

sending SCAN_REQ in the anchor node is periodically and randomly generated between 4750 to 5250 μs rather than a fixed value at 5000 μs as presented in the previous experiment. The scanning interval in a tag is unchanged. Figure 6.9 shows an example of generated random intervals (note that actual values are more diverse than these generated random intervals).

	Anchor node : Sending SCAN_REQ/ Receiving SCAN_RSP																		
Channel	CH37	CH38	CH39	CH37	CH38	CH39	CH37	CH38	CH39	CH37	CH38	CH39	CH37	CH38	CH39	CH37	CH38	CH39	so on…
time (μs)	5131	5027	5196	5160	4942	5222	5058	4936	5226	5042	5205	5058	5205	4940	4971	4921	4790	5045	

Figure 6.9 Randomly generated interval between 4750 μs and 5250 μs of anchor node for sending SCAN_REQ and receiving SCAN_RSP.

The results from this experiment based on the generated random intervals are shown in Table 6.2. It can be seen that the response rate is quite uniform along the distance and also uniformly distributed in each anchor node.

Table 6.2 Packet response rate with random scan interval.

Anchor Node ID	Response Rate (samples/sec)		
	1.5m (Trial 1)	1.5m (Trial 2)	3.0m
1	47.84	46.37	46.57
2	47.15	45.12	46.35
3	46.93	45.66	45.92
4	47.93	45.50	46.61
Total	**189.86**	**182.66**	**185.45**

All results in this experiment are subjected to four anchor nodes. If more nodes are introduced, the response rate will decrease accordingly.

6.3 Kalman Filter Test

The test in this section is to investigate the observed and filtered values using Kalman filter. The devices are place initially 3m apart. Then, one device is moved to 5m for a while, and it is then moved back to the original position. The process noise (R) and measurement noise (Q) in this work are set to 0.01 and 0.50, respectively. The sampling rate of the observed RTT is 1 sample per second.
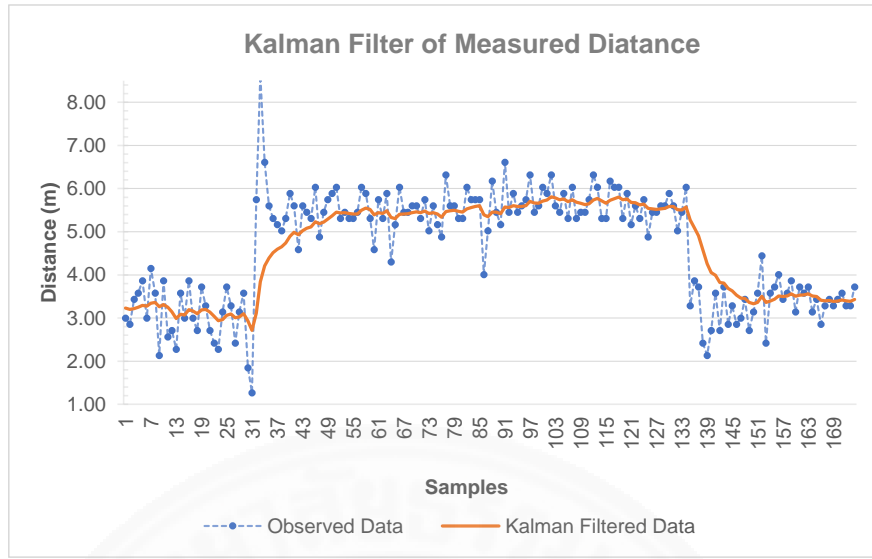
Figure 6.10 Kalman filter of measured distance.

Results in Figure 6.10 show that the filtered values are very well estimated, and the response to immediately change in a position is quick. The transition takes a few seconds to the new location.

6.4 Positioning Test

The test in this section is conducted in an L-shape living room with four anchor nodes attached at a mid-length of the selected walls. Six test points named TP1 through TP6 are designated for a tag location in order to observe data. The coordinates of the testing room, anchor nodes and a tag are illustrated in Figure 6.11. The RTT measurement requires a number of data for determining the estimated distance. Regarding to the experiment in section 6.2, the data acquisition rate for each anchor node is approximately 45 to 48 samples per second. Therefore, this work will perform averaging measured data if the number of data is greater than 50 samples. The average value is then filtered using Kalman algorithm with parameters given in section 6.3. Concurrently, recent filtered data will be sent to the back-end server for storing into the database, computing position as well as displaying on the web application in every second. The two positioning techniques are employed in the thesis. The geometric centroid of inner intersection area is considered first. The algorithm is modified from the work in [20]. It gives a good result when circles are intersect to each other, but no solution is available if no intersection. Therefore, the second positioning technique is

38

taken into account which is the Levenburg-marquardt algorithm. The algorithm always gives an optimal result.

Two experiments are investigated in following sections regarding to the condition of tag movement — a stationary and moving tag.
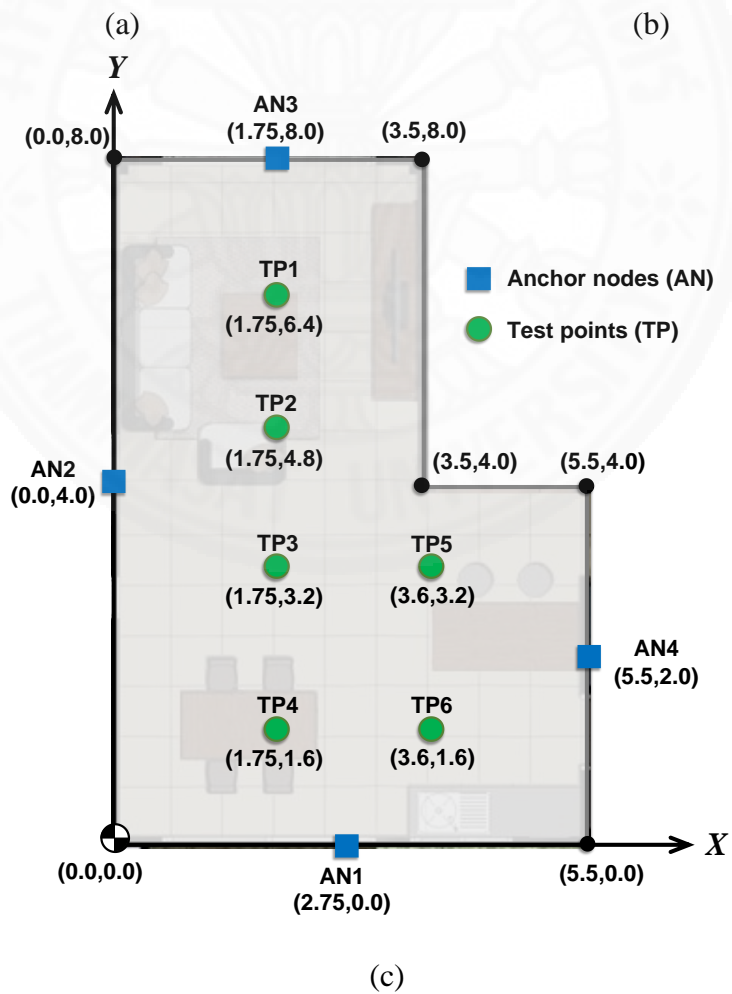

(a)   (b)

(c)

Figure 6.11 Testing room. (a) and (b) are Anchor nodes installation. (c) Plan with coordinates of room's corner, anchor nodes, and testing points.

39

6.4.1 Stationary Tag

A tag was placed at six stationary test points (TP1 through TP6) for 3 minutes and the results are shown in Figure 6.12.
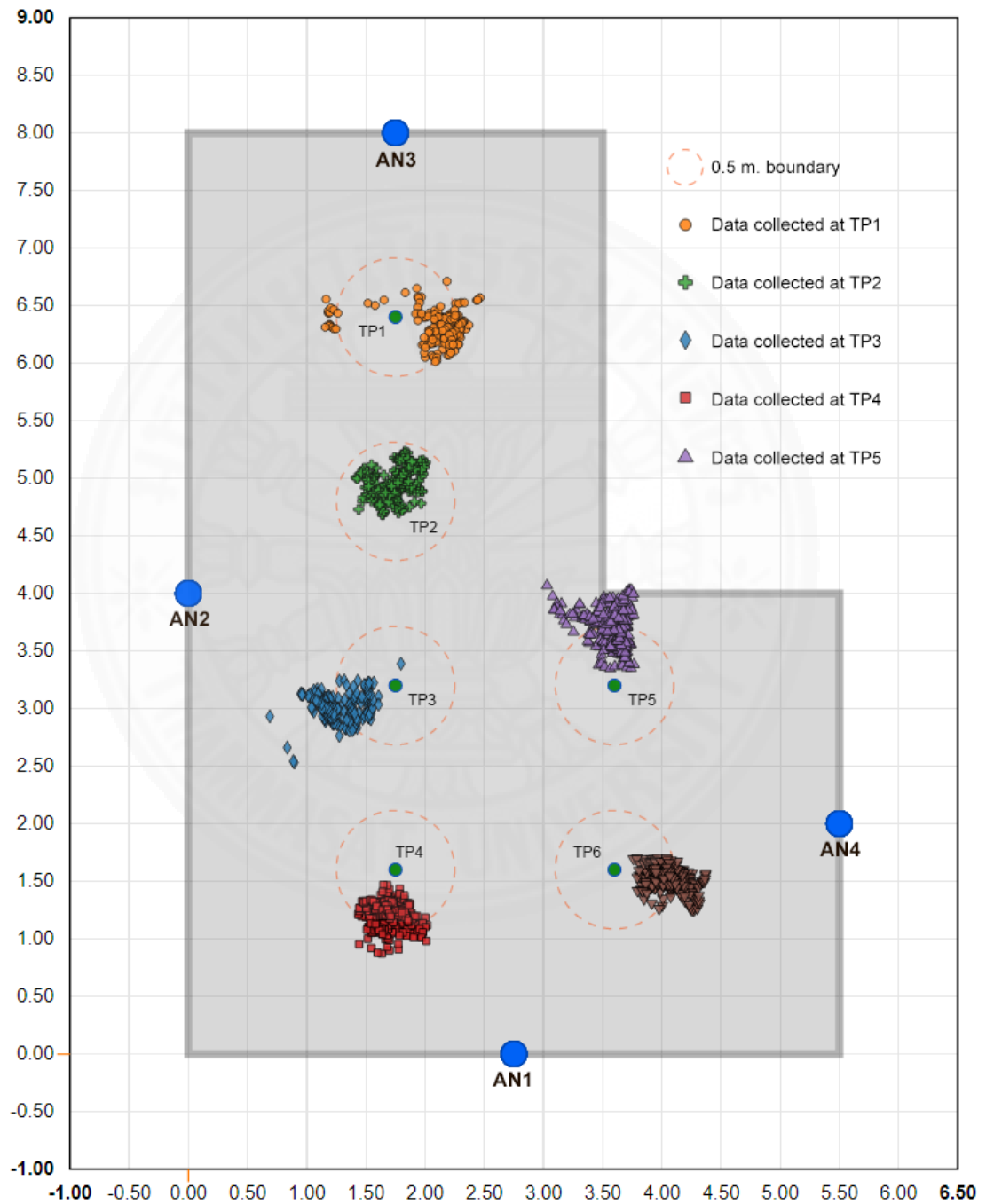

Figure 6.12 Stationary tag testing results.

Obviously, the computed positions give a good estimation. The deviations of computed positions from their centroid and from associated test point are shown in Table 6.3.

Table 6.3 Deviations of computed positions.

| Test Point	Test Point Coordinates (m)	Centroid of computed positions (m)	Deviations of centroid from associated test point (m)	Maximum deviation of computed positions from its centroid (m)	Maximum deviation of computed positions from associated test point (m)
TP1	(1.75, 6.40)	(2.09, 6.31)	0.35	0.95	0.73
TP2	(1.75, 4.80)	(1.72, 4.94)	0.15	0.36	0.44
TP3	(1.75, 3.20)	(1.27, 3.02)	0.51	0.64	1.10
TP4	(1.75, 1.60)	(1.68, 1.19)	0.42	0.39	0.74
TP5	(3.60, 3.20)	(3.56, 3.70)	0.51	0.65	1.05
TP6	(3.60, 1.60)	(4.05, 1.51)	0.46	0.36	0.78

Regarding to the above table, the computed positions are scattering at most 0.95m from their centroid (at TP1) and 1.10m from associated test point (at TP3). Moreover, the centroid of each group deviates from associated test point at most 0.51m. As mentioned previously, two trilateration algorithm are considered. Figure 6.13 demonstrates the input circles for the trilateration calculation and algorithm used in each test point. The positioning technique using the centroid of intersection area algorithm is applied to Figure 6.13(a), (b), (e) and (f) since at least three circles are intersect with each other. The Levenburg-marquardt positioning technique is applied to Figure 6.13(c) and (d).
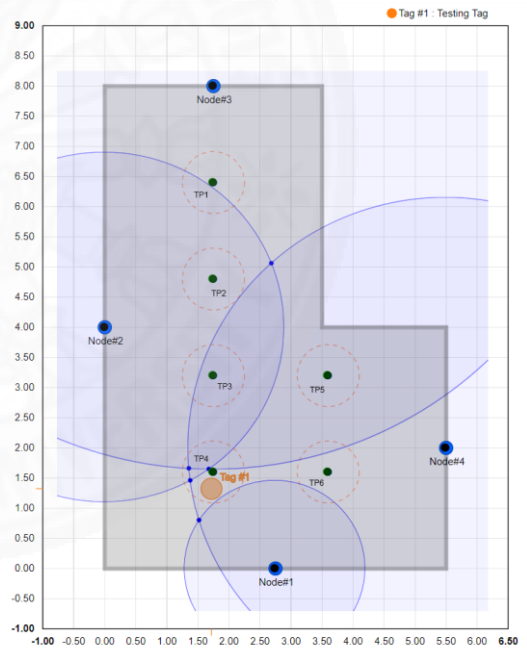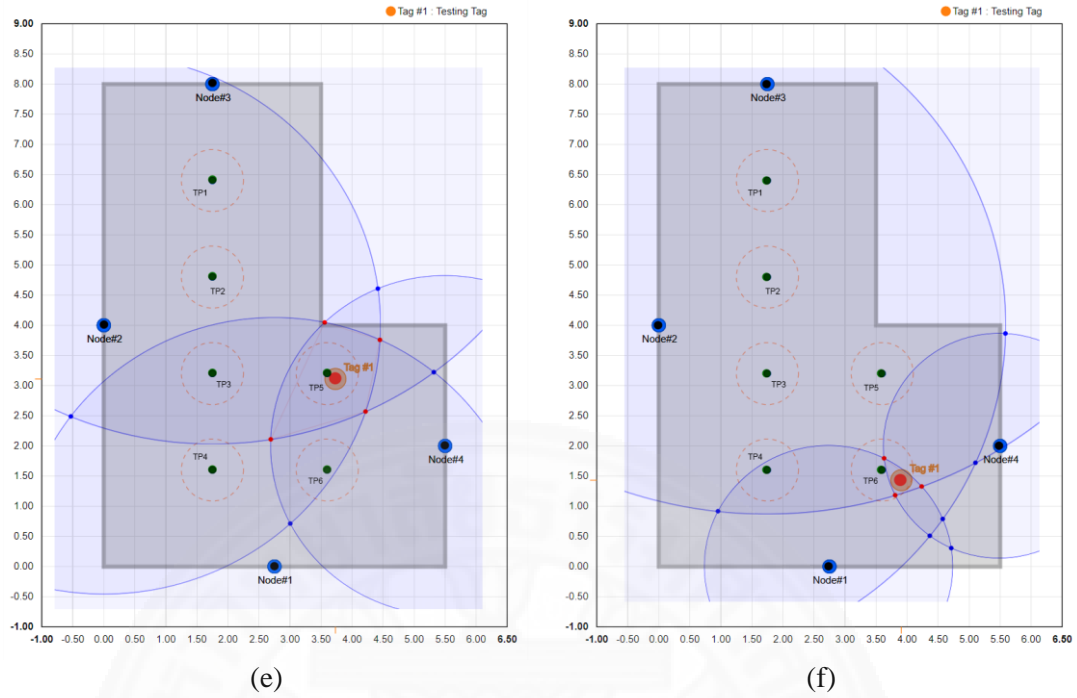
41

(a)

(b)

(c)

(d)

42

(e)   (f)
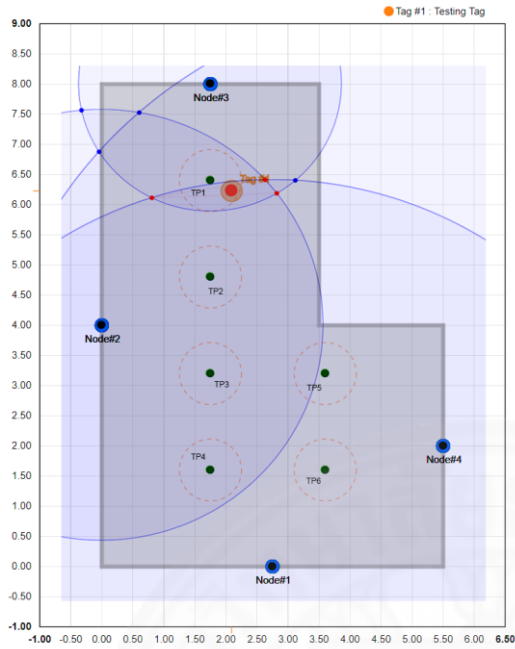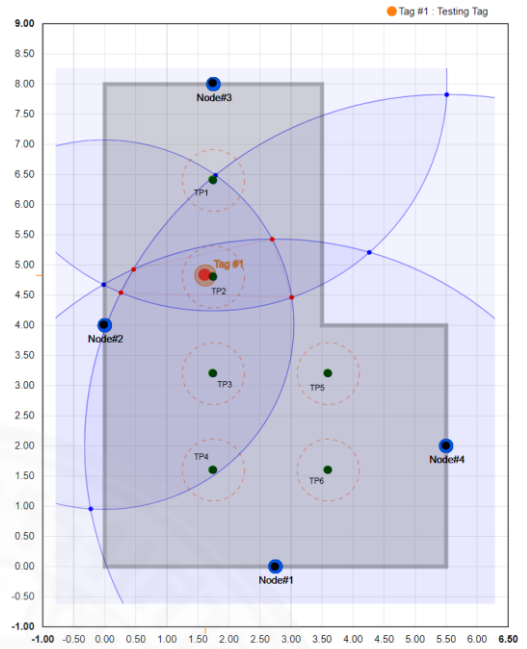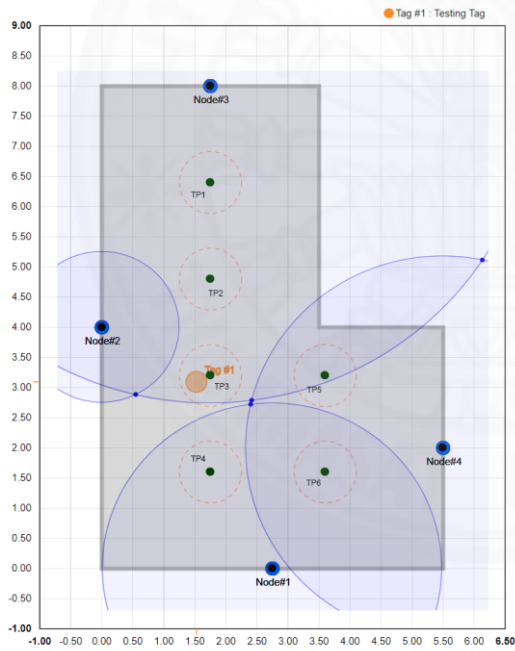
Figure 6.13 Example trilaterlation circles of each test point. (a) to (f) are results from TP1 to TP6, respectively.

6.4.2 Moving Tag

A tag in this test is moved from one test point to another, which starts from TP1 to TP6 in order. After reaching to the destination test point, a tag is left for approximately 30 seconds, and then it is moved to the next test point. The computed positions are plotted in Figure 6.14 and the perpendicular deviations from the computed positions to a moving path are also illustrated in Figure 6.15. The number of data between the test points is equal to the number of seconds since the system output is at every second. Results show that the proposed positioning system is quite responsive. It takes less than 10 seconds to reach the destination. The maximum deviation from the moving path is 0.99 meter while moving from TP3 to TP4.
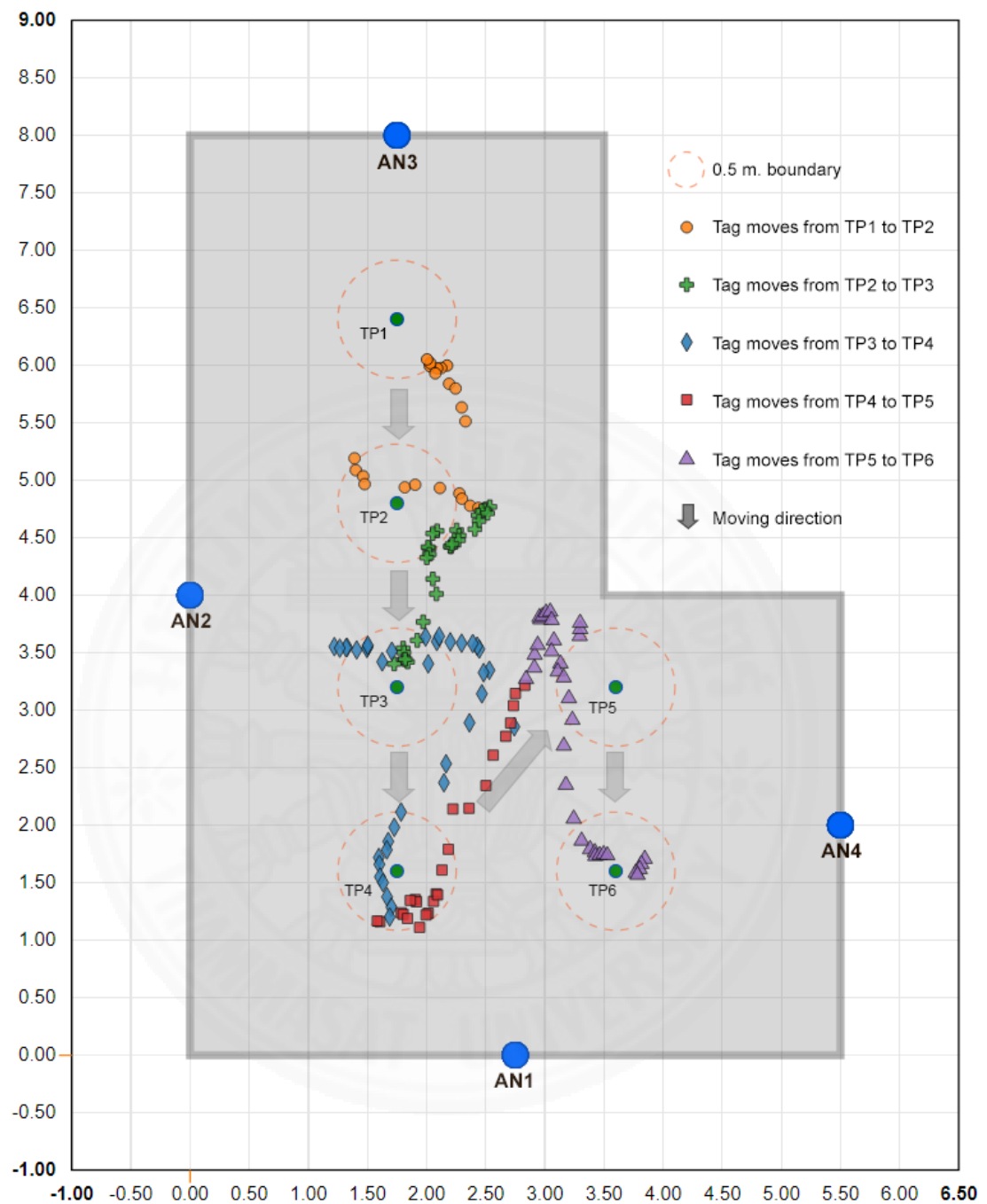
43

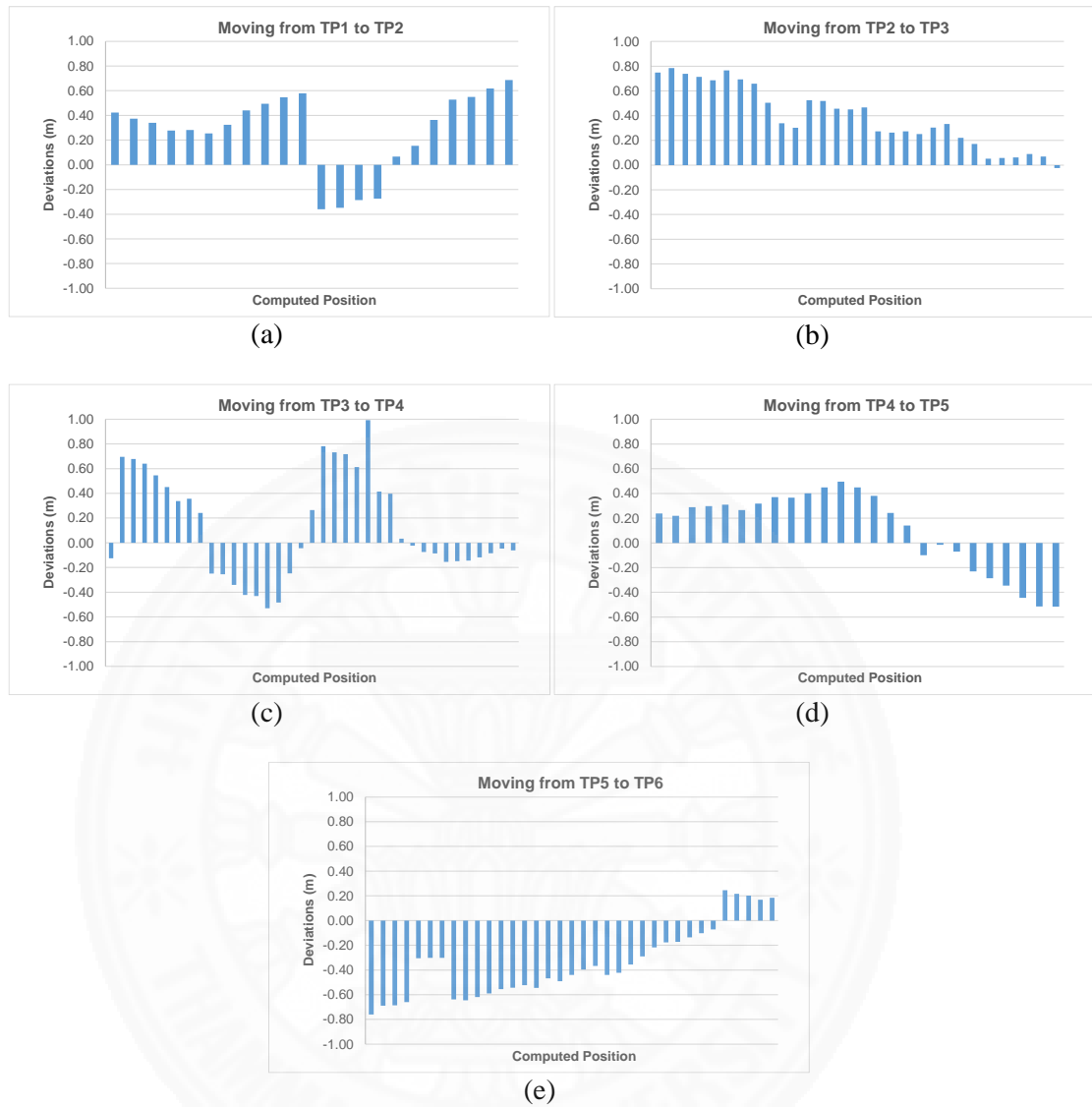Figure 6.14 Moving tag testing results.

Figure 6.15 The perpendicular deviations from the computed positions to a moving path**.**

Chapter 7

Conclusions

7.1 Conclusions

The indoor localization system based on pseudo-ranging from the RTT of BLE beacon has been proposed in this thesis. The system consists of four anchor nodes and one tag. It begins with the pseudo-ranging process, and then sends results to the back-end server to compute the position using the trilateration procedure. The results are then displayed on the application in real-time. Several services have been implemented to handle various tasks in this application framework. In the pseudo-ranging step, the RTT of the BLE beacon was measured by the CPU clock cycles generated by TCXO. Even though the clock runs at low frequency, the accuracy can still be achieved by the statistical approach. The RSSI is also utilized in order to improve the estimation accuracy of the RTT associated with the distance. The results show that the relationship between the distance and the RTT tends to be linear. The equation representing the RTT-distance relationship is derived for a later use. A sufficiently large number of RTT samples need to be collected to provide statistically meaningful average value for the distance estimation, and therefore every anchor nodes have to send request as much as possible. Consequently, the packets collision problem arises. By scheduling the scan request interval of anchor nodes randomly, the higher packet response rate can be achieved. The response rate is relatively equal in every anchor node with approximately 45 to 48 samples per second. Kalman filter is also introduced in this work to smoothen the estimated distances and the filtered results are well estimated and responsive. In the trilateration step, the centroid of inner intersection area positioning technique is firstly considered. If no solution found, the Levenburg-Marquardt algorithm is then taken into account. The results from the positioning test of a stationary tag show that the center of computed positions deviates at most 0.51 meter from associated test point, and the positions are scattering within 1 meter from their centers. Finally, the results from the moving tag experiment show that the deviation from the moving path is also less than 1 meter, and the transition from one to another test point takes less than 10 seconds.

7.2 Further Study

        The most important part of this work is the resolution of the clock. In other words, the speed of CPU. If the resolution is higher, the number required for sampling is less and the frequency for updating the computed position can be increased. The study using a newer chip from the same vendor named nRF52832, which has a higher clock speed, has been investigated. This chip is an Arm Cortex-M4 running 64 MHz, which gives a higher clock resolution than its predecessor. However, the RADIO peripheral still operates at 16 MHz. Therefore, the clock resolution is constrained by its RF front-end module. The new BLE chip having a higher RADIO peripheral clock is preferable and under an investigation.

References

[1]   Bluetooth SIG, *Bluetooth Core Specification v4.2*. 2014.

[2]   Y. Wang, X. Yang, Y. Zhao, Y. Liu, and L. Cuthbert, "Bluetooth positioning using RSSI and triangulation methods," *2013 IEEE 10th Consum. Commun. Netw. Conf. CCNC 2013*, pp. 837–842, 2013.

[3]   R. Mautz, "Indoor Positioning Technologies," *Inst. Geod. Photogramm. Dep. Civil, Environ. Geomat. Eng. ETH Zurich*, no. February 2012, p. 127, 2012.

[4]   H. Liu, H. Darabi, P. Banerjee, and J. Liu, "Survey of Wireless Indoor Positioning Techniques ans Systems," *IEEE Trans. Syst. Man Cybern. C Appl. Rev.*, vol. 37, no. 6, pp. 1067–1080, 2007.

[5]   Y. Gu, A. Lo, and I. Niemegeers, "A survey of indoor positioning systems for wireless personal networks," *IEEE Commun. Surv. Tutorials*, vol. 11, no. 1, pp. 13–32, 2009.

[6]   M. E. Rida, F. Liu, Y. Jadi, A. A. A. Algawhari, and A. Askourih, "Indoor Location Position Based on Bluetooth Signal Strength," *2015 2nd Int. Conf. Inf. Sci. Control Eng.*, pp. 769–773, 2015.

[7]   Q. Dong and W. Dargie, "Evaluation of the reliability of RSSI for indoor localization," *2012 Int. Conf. Wirel. Commun. Undergr. Confin. Areas, ICWCUCA 2012*, pp. 2–7, 2012.

[8]   R. Faragher and R. Harle, "Location Fingerprinting With Bluetooth Low Energy Beacons," *IEEE J. Sel. Areas Commun.*, vol. 33, no. 11, pp. 2418–2428, 2015.

[9]   M. L. Rodrigues, L. F. M. Vieira, and M. F. M. Campos, "Fingerprinting-based radio localization in indoor environments using multiple wireless technologies," *IEEE Int. Symp. Pers. Indoor Mob. Radio Commun. PIMRC*, pp. 1203–1207, 2011.

[10]   S. Park, H. S. Ahn, and W. Yu, "Round-trip time-based wireless positioning without time synchronization," *ICCAS 2007 - Int. Conf. Control. Autom. Syst.*, pp. 2323–2326, 2007.

[11]   I. Casacuberta and A. Ramirez, "Time-of-flight Positioning Using the Existing Wireless Local Area Network Infrastructure," in *Proceedings of International Conference on Indoor Positioning and Indoor Navigation*, 2012, pp. 1–8.

[12] W. S. Murphy, "Determination of a Position Using Approximate Distances and Trilateration," Thesis (M. Sc.), Colorado School of Mines, 1992.

[13] M. I. a Lourakis, "A Brief Description of the Levenberg-Marquardt Algorithm Implemened by levmar," *Matrix*, vol. 3, p. 2, 2005.

[14] Nordic Semiconductor ASA, "nRF51822 - Bluetooth Low Energy Products." [Online]. Available: https://www.nordicsemi.com/eng/Products/Bluetooth-low-energy/nRF51822.

[15] Nordic Semiconductor ASA, "nRF51822 Product Specification v3.3," 2016.

[16] Nordic Semiconductor ASA, "nRF51 Series Reference Manual," 2014.

[17] Nordic Semiconductor ASA, "S132 SoftDevice Specification v3.0," 2016.

[18] M. S. Grewal and A. P. Andrews, *Kalman filtering: Theory and Practice using Matlab*, 4th ed. John Wiley & Sons, Inc., 2015.

[19] G. Welch and G. Bishop, "An Introduction to the Kalman Filter," *In Pract.*, vol. 7, no. 1, pp. 1–16, 2006.

[20] "Trilateration." [Online]. Available: https://github.com/noomrevlis/trilateration.

Appendix

Appendix A

TCXO Specification

A.1 High Precision TCXO specification 16.000MHz

parameter	character	technical parameters	unit
output	working frequency	16.0000	MHz
	frequency accuracy	±0.1Maxnormal temperature 25°C	ppm
	Waveform (square wave/sine wave)	square wave (COMS/TTL)	
	phase noise	-110dbc/100Hz -130dbc/1KHz -145dbc/10KHz	
	Increase/decrease time (square)）	10	ns
temperature characteristic	temperature characteristic	±1/-20-70°C	ppm
aging rate	aging rate/year	1 Max	ppm
power supply	supply voltage	3-5v	VDC
	working current	30 Max	mA
	Load regulation	±0.2 Max	ppm
other specifications	operating temperature	-20~+70	°C
	storage temperature	-40~+85	°C
	Overall dimensions	20.3*12.5*8	mm
	start time to oscillate	2msMax	
	output level"0"	0.4v/10%vdd Max	
	output level"1"	2.4v/90%vdd Min	
	output symmetry	50%Vdd/50%(duty cycle)	
	output load	15PF/10TTL	

MODEL : GE
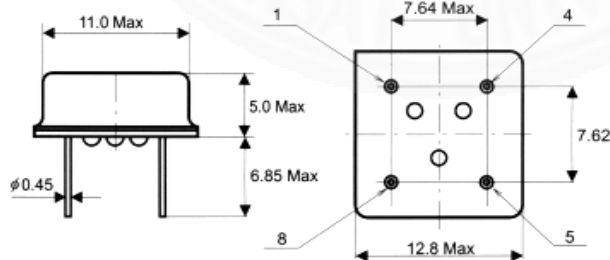
Pin functions
1: NC
4: GND
5: OUT
8:VC（3v-5v）